

# Deliberation gated by opportunity cost adapts to context with urgency

Maximilian Puelma Touzel,<sup>1,2,\*</sup> Paul Cisek,<sup>3</sup> and Guillaume Lajoie<sup>1,4,5</sup>

<sup>1</sup>*Mila, Quebec AI Institute*

<sup>2</sup>*Department of Computer Science and Operations Research, Université de Montréal*

<sup>3</sup>*Department of Neuroscience, Université de Montréal*

<sup>4</sup>*Department of Mathematics and Statistics, Université de Montréal*

<sup>5</sup>*Canada CIFAR AI Chair*

## Abstract

The value we place on our time impacts what we decide to do with it. Value it too little, and we obsess over all details. Value it too much, and we rush carelessly to move on. How to strike this often context-specific balance is a challenging decision-making problem. Average-reward, putatively encoded by tonic dopamine, serves in existing reinforcement learning theory as the stationary opportunity cost of time. However, environmental context and the cost of deliberation therein often varies in time and is hard to infer and predict. Here, we define a non-stationary opportunity cost of deliberation arising from performance variation on multiple timescales. Estimated from reward history, this cost readily adapts to reward-relevant changes in context and suggests a generalization of average-reward reinforcement learning (AR-RL) to account for non-stationary contextual factors. We use this deliberation cost in a simple decision-making heuristic called *Performance-Gated Deliberation*, which approximates AR-RL and is consistent with empirical results in both cognitive and systems decision-making neuroscience. We propose that deliberation cost is implemented directly as urgency, a previously characterized neural signal effectively controlling the speed of the decision-making process. We use behaviour and neural recordings from non-human primates in a non-stationary random walk prediction task to support our results. We make readily testable predictions for both neural activity and behaviour and discuss how this proposal can facilitate future work in cognitive and systems neuroscience of reward-driven behaviour.

Keywords: primate decision-making, reinforcement learning, urgency, opportunity cost

---

\* [puelmatm@mila.quebec](mailto:puelmatm@mila.quebec)

symbol	quantity
$t$	within-trial time
$k$	trial index
$S_t$	within-trial state at time $t$
$\mathbf{S}_t$	state sequence up to time $t$
$R_k$	reward of $k$ th trial
$T_k$	duration of $k$ th trial
$t_k^{\text{dec}}$	decision time of $k$ th trial
$C_t^{\text{del}}$	within-trial opportunity cost of deliberation
$r_{\text{max}}$	maximum reward achievable in a trial
$b_t$	belief of correct report given $\mathbf{S}_t$
$\bar{r}_t$	expected reward for reporting at time $t$
$C_t^{\text{com}}$	within-trial opportunity cost of commitment
$\rho$	stationary reward rate
$\rho^*$	optimal stationary reward rate
$\alpha$	context parameter
$\rho_\alpha$	context-conditioned stationary reward rate
$T_\alpha$	context-conditioned stationary average trial duration
$\hat{\rho}_k^\tau$	reward history filtered through a timescale, $\tau$
$\tau_{\text{long}}$	a long timescale over which to estimate $\rho$
$\tau_{\text{context}}$	a context-specific timescale over which to estimate $\rho_\alpha$
$\nu$	tracking cost sensitivity
$K$	subjective reward scale factor
$T_{\text{block}}$	characteristic duration of a trial block
$c$	auxiliary deliberation cost rate
$N_t$	tokens difference
$p$	jump probability of random walk, $p \geq 1/2$

Table I. Symbol glossary. Highlighted in gray are parameters of the PGD model presented in this paper.

10

## INTRODUCTION

11 Humans and other animals make a wide range of decisions throughout their daily lives.  
 12 Any particular action usually arises out of a hierarchy of decisions involving a careful balance  
 13 between resources, including one that is always limited: time. The cost of *spending* time  
 14 depends on its value, a construct that relies on comparing against the alternative things  
 15 an agent could potentially do with it. Estimating time's value is not straightforward for a  
 16 number of reasons. There are alternative choices at multiple decision levels, e.g. moving on  
 17 from a job and moving on from a career, and each level requires its own evaluation. Moreover,  
 18 the value of alternatives needs to be tracked as they may change over time depending on the  
 19 context in which a decision is made. For example, animals will learn to value a given food  
 20 resource differently depending on whether it is encountered during times of plenty versus  
 21 scarcity. The agent's knowledge of and ability to track context thus influences the value it  
 22 assigns to possible alternatives.

23 These are significant, practical complications of making decisions contingent on *opportu-*

24 *nity costs* [1], the formal economic concept capturing the value of the alternatives lost by  
25 committing a limited resource to a given use. The opportunity cost of time is neverthe-  
26 less well-studied in decision-making theory for relative definitions of value, most notably as  
27 the average reward in average-reward reinforcement learning (AR-RL) [2]. AR-RL focuses  
28 on deviations from the average reward rather than on discounted reward as in the more  
29 widely known discount-reward reinforcement learning formulation. In neuroscience, AR-RL  
30 was first proposed to extend the reward prediction error hypothesis for phasic dopamine  
31 to account also for the observed properties of tonic dopamine levels [3]. It has since been  
32 used to emphasize the relative nature of reward-based decision-making [4] in explanations  
33 of human and animal behaviour in foraging [5], free-operant conditioning [6], perceptual  
34 decision-making [7, 8], cognitive effort/control [8, 9], and even economic exchange [10].

35 AR-RL is increasingly acknowledged as the more suitable reinforcement learning formu-  
36 lation [11] for *continuing environments* in which there is no definite end [12], in a large part  
37 because it explicitly seeks solutions that achieve the maximum possible average reward rate.  
38 This is in contrast to traditional fixed accuracy criteria in perceptual decision-making tasks  
39 that focus on maximizing trial reward alone [13]. The solutions to AR-RL formulations of  
40 tasks of long sequence of trials are decision boundaries in the state space of a trial that  
41 typically collapse with trial time. This limits deliberation in trials with low return-on-time-  
42 investment, e.g. in difficult trials for tasks in which trial difficulty is variable [7, 14].

43 Up to now, however, AR-RL and most of its applications have focused on fixed context  
44 and have used the stationary average reward as the fixed opportunity cost of time, which  
45 ignores context-dependent performance variation. This is perhaps not surprising given that  
46 in psychological and neuroscientific studies of decision-making, we usually eliminate such  
47 contextual factors from the experimental design such that our models describe stationary  
48 behaviour. However, the brain mechanisms under study are adapted to a more diverse  
49 natural world in which contextual factors are often relevant, hard to infer and vary over  
50 time [4].

51 We pursue a theory of approximate relative-value decision-making under uncertainty in a  
52 setting relevant to decision-making neuroscience. We start by showing that value in AR-RL  
53 can be expressed using the opportunity costs of deliberation and commitment. Here, the  
54 commitment cost is the shortfall in reward relative to the maximum possible in a trial that  
55 is expected to be lost when committing to a decision at a given time. Highlighting the risk  
56 of value representations in non-stationary environments, we propose an approximation to  
57 the AR-RL value-optimal solution, Performance-Gated Deliberation (PGD), that uses the  
58 opportunity cost directly as the collapsing decision boundary, instead of as input to a value  
59 optimization problem. PGD thus reduces decision-making to estimating two opportunity  
60 costs: a commitment cost learned from the statistics of the environment and a deliberation  
61 cost estimated from tracking one’s own performance in that environment. It explains how an  
62 agent, without explicitly tracking context parameters or storing a value function, can trade-  
63 off speed and accuracy according to performance at the typically longer timescales over which  
64 context changes. We propose that deliberation cost is then directly encoded as “urgency”  
65 in the neural dynamics underlying decision-making [7, 15–17]. The theory is thus directly  
66 testable using both behaviour and neural recordings. To illustrate how PGD applies in a  
67 specific continuing decision-making task, and to make the links to a neural implementation  
68 explicit, we analyze behavior and neural recordings collected over eight years from two non-  
69 human primates (NHPs) [18, 19]. They performed successive trials of the “tokens task”,  
70 a probabilistic guessing task in which information about the correct choice is continuously

71 changing within each trial, and a task parameter controlling the incentive to decide early  
72 (the context) is varied over longer timescales. Behavior in the task, in both humans [16]  
73 and monkeys [19], provides additional support to an existing hypothesis about how neural  
74 dynamics implements time-sensitive decision-making [15]. Specifically, neural recordings in  
75 monkeys suggest that the evidence needed to make the decision predominates in dorsolateral  
76 prefrontal cortex [20]; a growing context-dependent urgency signal is provided by the basal  
77 ganglia [21]; and the two are combined to bias and time, respectively, a competition between  
78 potential actions that unfolds in dorsal premotor and primary motor cortex [18]. Similar  
79 findings have been reported in other tasks - for example, in the frontal eye fields during  
80 decisions about eye-movements [17]. PGD is proposed as the theoretical explanation for  
81 why decision-making mechanisms are organized in this way. As an algorithm, it serves as a  
82 robust means to balance immediate rewards and the cost of time across multiple timescales.  
83 As a quantitative model, it serves to explain concurrently recorded behaviour and neural  
84 urgency in continuing decision-making tasks.

## 85 RESULTS

### 86 A. Theory of performance-gated deliberation

#### 87 1. Opportunity costs of deliberation and commitment, and drawbacks of average-reward 88 reinforcement learning

89 We consider a class of tasks consisting of a long sequence of trials indexed by  $k =$   
90  $1, 2, \dots$  (see fig. 1a), each of which provides the opportunity to obtain some reward by choos-  
91 ing correctly. In each trial, a finite sequence of states,  $S_t$ ,  $t = 0, \dots, t_{\max}$ , is observed that  
92 provide evidence for an evolving belief about the correct choice among a fixed set of options.  
93 To keep notation simple, we suppress denoting the trial index,  $k$ , on quantities such as trial  
94 state,  $S_t$ , that also depend on trial time,  $t$ . The time of decision,  $t_k^{\text{dec}}$ , and the chosen option  
95 determine both the reward received,  $R_k$ , and the trial duration,  $T_k \geq t_k^{\text{dec}}$ . Importantly,  
96 decision timing can affect performance because earlier decisions typically lead to shorter  
97 trials (and thus more trials in a given time window), while later decisions lead to higher  
98 accuracy. Effectively balancing such speed-accuracy trade-offs is central to performing well  
99 in continuing episodic task settings. For a fixed strategy, the *stationary reward rate* (see  
100 slope of dashed line in fig. 1a(right)) is  
101

$$\rho := \lim_{k \rightarrow \infty} \frac{\sum_k R_k}{\sum_k T_k}. \quad (1)$$

102 For a stochastic environment, the definition of  $\rho$  includes an ensemble average. Free-operant  
103 conditioning, foraging, and several perceptual decision-making tasks often fall into this class.  
104 Previous work [7, 22] has studied the belief of correct report for binary rewards,  $b_t = P(R_k =$   
105  $1 | \mathcal{S}_t, t^{\text{dec}} = t)$ , which also gives the expected trial reward,  $\bar{r}_t = b_t \cdot 1 + (1 - b_t) \cdot 0 = b_t$  [7]  
106 (see [23] for more about the relationship between value-based and perceptual decisions).  $\mathcal{S}_t$   
107 denotes the state sequence observed so far,  $(S_0, \dots, S_t)$ . We consider greedy strategies that  
108 report the choice with the largest belief at decision time. The decision problem is then about  
109 *when* to decide.

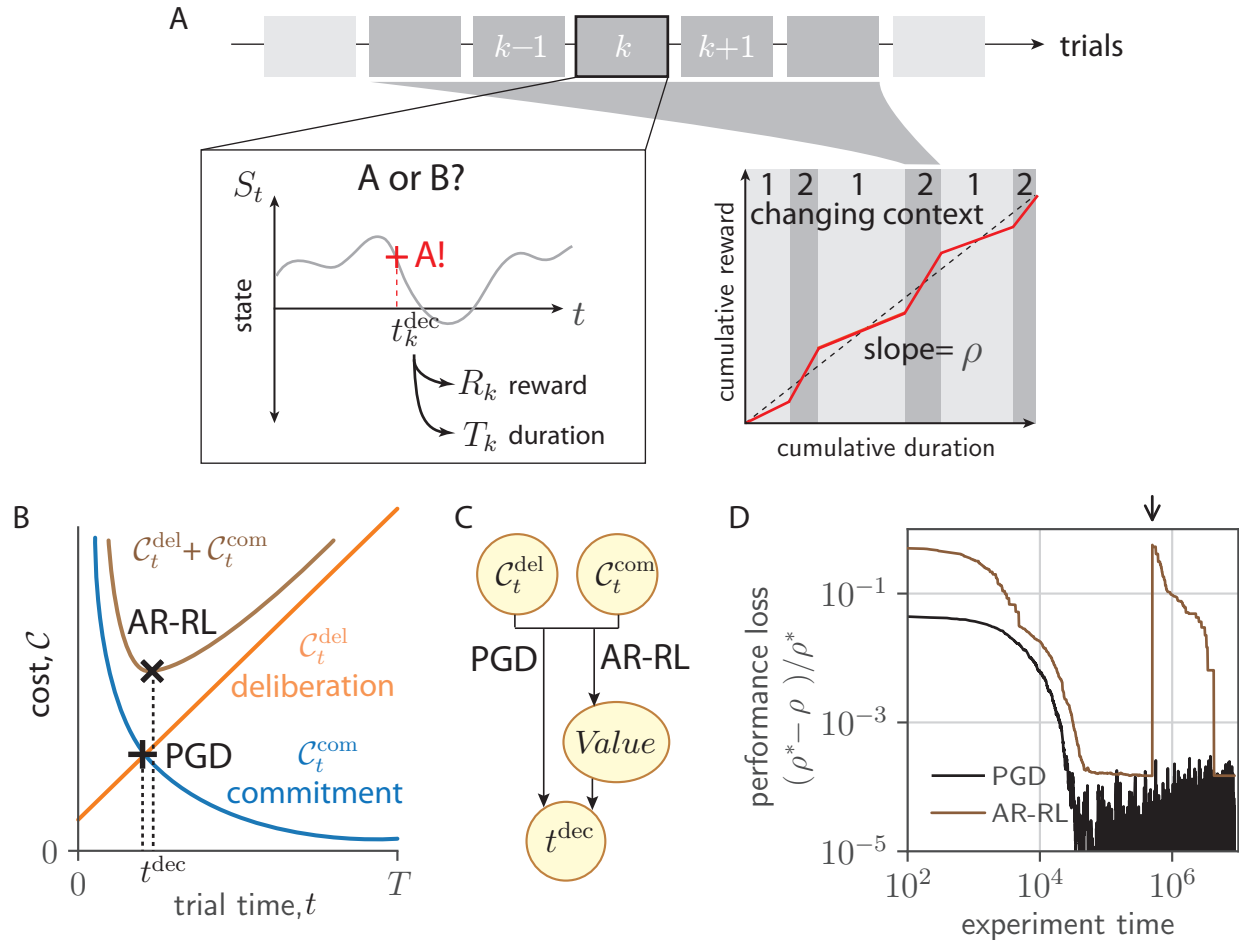


Figure 1. *AR-RL and Performance-Gated Deliberation*. (a) Task setting. Left: Within trial state,  $S_t$  evolves over trial time  $t$  in successive trials indexed by  $k$ . The decision ‘A’ is reported at the decision time  $t_k^{\text{dec}}$  (red cross), determining trial reward,  $R_k$ , and trial duration,  $T_k$ . Right: Sketch of cumulative reward versus cumulative duration. Context-conditioned reward rate (slope of red line), varies with alternating context (labelled 1 and 2) around average reward,  $\rho$  (dashed line). (b) Decision rules based on opportunity costs of commitment,  $C_t^{\text{com}}$ , and deliberation,  $C_t^{\text{del}}$ . The AR-RL rule (black ‘x’) finds  $t$  that minimizes  $C_t^{\text{del}} + C_t^{\text{com}}$ . The PGD rule (black cross) finds  $t^{\text{dec}}$  at which they intersect,  $C_t^{\text{del}} = C_t^{\text{com}}$ . (c) Schematic diagram of each algorithm’s dependency. PGD computes a decision time directly from the two opportunity costs, while AR-RL uses both to first estimate a value function, whose maximum specifies the decision time. (d) Loss (error in performance with respect to the optimal policy,  $(\rho^* - \rho)/\rho^*$ ) over learning time in a patch-leaving task (AR-RL: brown, PGD: black). The arrow indicates when the state labels were randomly permuted.

110 Average-reward reinforcement learning (AR-RL), first proposed in artificial intelli-  
 111 gence [24], was later incorporated into reward prediction error theories of dopamine sig-  
 112 nalling [3] and employed to account for the opportunity cost of time [6]. AR-RL was  
 113 subsequently used to study reward-based decision-making in neuroscience and psychol-  
 114 ogy [7, 8, 25, 26]. AR-RL centers around the average-adjusted future return, which penalizes  
 115 the passage of time according the average reward. A reporting decision is associated with a  
 116 return that for trial-based tasks combines the remainder of the current trial and all future

117 trials,  $\bar{r}_t - \rho(T_k - t) + \sum_{k' > k} (R_{k'} - \rho T_{k'})$ , where  $\rho$  (*c.f.* eq. (1)) is either estimated online  
118 or obtained self-consistently (see [Methods](#) for details). Value is defined as the future return  
119 averaged over trial sequence realizations. This average of a sum of reward deviations into  
120 the future converges on account of the decaying effects of the state at which the decision is  
121 made. The AR-RL algorithms we consider aim to achieve the highest  $\rho$  by also maximizing  
122 the average-adjusted value. We now provide an alternative, but equivalent definition of  
123 average-adjusted trial return in terms of opportunity costs incurred by the agent.

124 We denote the opportunity cost of committing at time  $t$  within a trial as  $\mathcal{C}_t^{\text{com}}$ , defined  
125 as the difference

$$\mathcal{C}_t^{\text{com}} = r_{\max} - \bar{r}_t, \quad (2)$$

126 where  $r_{\max}$  is the maximum trial reward possible *a priori*. Within a trial, an agent lowers  
127 its commitment cost towards zero by accumulating more evidence, i.e. by waiting. Waiting,  
128 however, incurs another opportunity cost: the reward lost by not acting. We denote this  
129 opportunity cost of deliberation incurred up to a time  $t$  in a trial as  $\mathcal{C}_t^{\text{del}}$ . In AR-RL, the  
130 constant opportunity cost rate of time is integrated so that for  $T_k = t_k^{\text{dec}}$ ,

$$\mathcal{C}_t^{\text{del}} = \rho t. \quad (3)$$

131 With these definitions, the average-adjusted trial return for deciding at a time  $t$  can be  
132 expressed as  $r_{\max} - (\mathcal{C}_t^{\text{com}} + \mathcal{C}_t^{\text{del}})$ . It is maximized by jointly minimizing  $\mathcal{C}_t^{\text{del}}$  and  $\mathcal{C}_t^{\text{com}}$  ([fig. 1b](#)),  
133 giving the AR-RL optimal solution (see [Methods](#) for a formal statement and solution of the  
134 AR-RL problem). Expressed in this way, the average-adjusted trial return emphasizes the  
135 more general perspective that an agent's solution to the speed-accuracy trade-off is about  
136 how it balances the decaying opportunity cost of commitment and the growing opportunity  
137 cost of deliberation.

138 Despite their utility, value representations such as the average-adjusted trial return can  
139 be a liability in real world tasks where task statistics are non-stationary. To illustrate this,  
140 we consider the following foraging task. An foraging agent feeds among a fixed set of food  
141 (e.g. berry) patches. Total berries consumed in a patch saturates with duration  $t$  according  
142 to a given saturation profile, shared across patches, as the fewer berries left are harder to  
143 find. Patches differ in their richness (e.g. berry density), which is randomly sampled and  
144 fixed over the task. Denoting patch identity (serving as context) by  $s$ , the food return is  
145 directly observed and deterministic given  $s$ . To perform well, the agent needs to decide when  
146 to move on from depleting the current patch. Further details about the task and its solution  
147 are given in the [Methods](#). For a broad class of online AR-RL algorithms, the agent learns the  
148 average-adjusted trial return as a function of state and time. For a given patch, it then leaves  
149 when this return is at its maximum (*c.f.* [fig. 1b](#)). In [fig. 1d](#), we show how the performance  
150 (brown line) approaches that of the optimal policy in time as the estimation of the AR-RL  
151 trial return improves with experience (see [Methods](#) for implementation details). However, if  
152 the agent's environment undergoes a significant disturbance (e.g. a forest fire due to which  
153 the patch locations are effectively re-sampled), the performance of this AR-RL algorithm can  
154 drop back to where it started. We implement such a disturbance via random permutation  
155 of the state labels at the time indicated by the arrow in [fig. 1d](#). This is true over a range of  
156 learning rates and the number of patches ([fig. S8](#)). More generally, any approach that relies  
157 on estimating state-value associations shares this drawback, including those approaches that  
158 implicitly learn those associations by directly learning a policy instead [27]. Could context-  
159 dependent decision times be obtained without having to associate value or action to state?  
160 A means to do so is presented in the next section.



161

## 2. Performance-Gated Deliberation

162 We propose that instead of maximizing value as in AR-RL, which minimizes the sum of  
163 the two opportunity costs,  $\mathcal{C}_t^{\text{del}} + \mathcal{C}_t^{\text{com}}$ , the agent simply takes as its decision criterion when  
164 they intersect (shown as the black cross in [fig. 1b](#)).

$$t^{\text{dec}} := \min_t \{t \mid \mathcal{C}_t^{\text{del}} \geq \mathcal{C}_t^{\text{com}}\} \quad (\text{PGD decision rule}) \quad (4)$$

165 We call this heuristic rule at the center of our results *Performance-Gated Deliberation*  
166 (PGD). Plotted alongside the AR-RL performance in [fig. 1d](#) for our example foraging task,  
167 PGD (black line) achieves better performance than AR-RL overall. It is also insensitive to  
168 the applied disturbance since PGD uses  $\mathcal{C}_t^{\text{del}}$  and  $\mathcal{C}_t^{\text{com}}$  directly when deciding, rather than  
169 as input to problem of optimizing average-adjusted value as in AR-RL ([fig. 1c](#)).

170 We constructed the above task so that PGD is the AR-RL optimal solution. In general,  
171 however, PGD is a well-motivated approximation to the optimal strategy, so we call it a  
172 heuristic. In the more general stochastic setting where there is residual uncertainty in trial  
173 reward at decision time, the PGD agent will have to learn the association between state  
174 and expected reward,  $\bar{r}_t$ . This association is learned from within-trial correlations only. In  
175 contrast, the opportunity cost of time as the basis for the deliberation cost depends on  
176 across-trial correlations that together determine the overall performance. It is thus more  
177 susceptible to non-stationarity. A typical task setting is when the value of the same low-level  
178 action plan differs across context. From hereon, we will assume the agent has learned the  
179 stationary opportunity cost of commitment and so focus on resolving the remaining problem:  
180 how to learn and use an opportunity cost of deliberation that exhibits non-stationarity on  
181 the longer timescales over which context varies.

182

## 3. Reward filtering for a dynamic opportunity cost of deliberation

183 The state disturbance in the toy example above altered task statistics at only a single  
184 time point. In general, however, changes in task statistics over time can occur throughout  
185 the task experience. A broader notion of deliberation cost beyond the static average reward  
186 is thus needed—one that can account for extended timescales over which performance varies.  
187 Such a cost serves as a dynamic reference in a relative definition of value based on a non-  
188 stationary opportunity cost of time. We first address how performance on various timescales  
189 can be estimated.

190 As a concrete example, we make use of the task that we will present in detail in the fol-  
191 lowing section. This task has a context parameter,  $\alpha$ , that can vary in time on characteristic  
192 timescales longer than the moment-to-moment and can serve as a source of non-stationarity  
193 in performance. Here, the context sequence,  $\alpha_k$ , varies on a single timescale, e.g. through pe-  
194 riodic switching between two values. The resulting performance ([fig. 2a\(top\)](#)) varies around  
195 the stationary average,  $\rho$  (purple), with context variation due to the switching (orange), as  
196 well as context-conditioned trial-to-trial variation (blue). The decomposition of time-varying  
197 performance into these multiple, timescale-specific components can be achieved by passing  
198 the reward signal through parallel filters, each designed to retain the signal variation specific  
199 to that timescale ([fig. 2a\(bottom\)](#)). There are multiple approaches to this decomposition.  
200 We chose a heuristic approach in which the performance over a finite memory timescale can  
201 be estimated by filtering the sequence of rewards through a simple low-pass filter [[8](#), [28](#)].

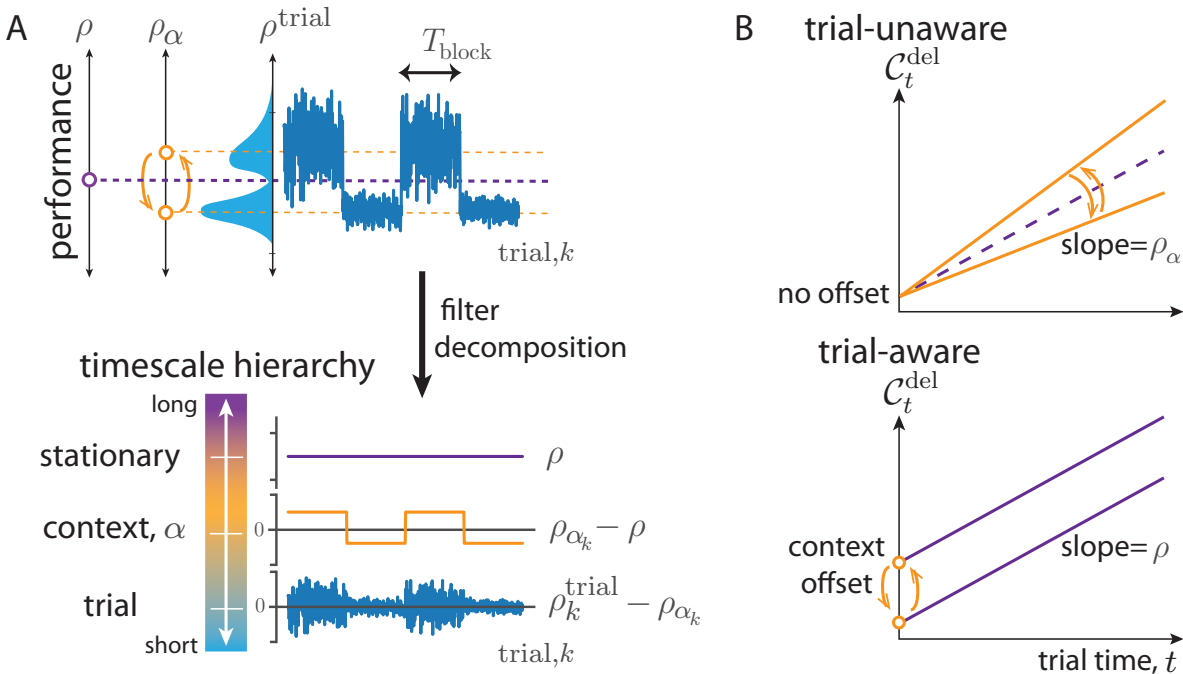


Figure 2. *Non-stationary opportunity cost.* (a) Top: Dynamics of trial performance ( $\rho_k^{\text{trial}} := R_k/T_k$ ; blue) with its distribution as well as dynamics of between context-conditioned averages of performance ( $\rho_\alpha = \langle \rho_k^{\text{trial}} \rangle_{k|\alpha}$ ; orange), and the effectively stationary average performance ( $\rho \sim \langle \rho_k^{\text{trial}} \rangle_k$ ; purple). Bottom: these are decomposed into a hierarchy by filtering reward history on trial, context, and long timescales, respectively. (b) Two hypothetical forms for context-specific trial opportunity cost. Top: Trial-unaware cost in which context varies the slope around  $\rho$ . Bottom: Trial-aware cost in which context variation is through a bias ( eq. (5)).

202 This filter is defined by an integration time,  $\tau$ , tuned to trade off the bias and variance  
 203 of the estimate in order to best capture the variation on the desired timescale (e.g. how  
 204 performance varies over different contexts). We denote such an estimate  $\hat{\rho}_k^\tau$ , and show in  
 205 the [Methods](#) that it approximates the average reward over the last  $\tau$  time units. We discuss  
 206 the question of biological implementation in the discussion, but note here that the number  
 207 and values of  $\tau$  needed to represent performance variation in a given task could be learned  
 208 or selected from a more complete set in an online fashion during task learning. In an exper-  
 209 imental setting, these learned values can in principle be inferred from observed behaviour  
 210 and we developed such an approach in the analysis of data that we present in the following  
 211 section.

212 Applying this heuristic decomposition here, the stationary reward rate,  $\rho$ , can be esti-  
 213 mated to high precision by using a long integration time,  $\tau_{\text{long}}$ , to the reward sequence  $R_k$ ,  
 214 producing the estimate  $\hat{\rho}_k^{\tau_{\text{long}}}$ . If  $\alpha_k$  were a constant sequence,  $C_t^{\text{del}} = \hat{\rho}_k^{\tau_{\text{long}}} t$ , the station-  
 215 ary opportunity cost of deliberation eq. (3) of AR-RL. However, in this example context  
 216 varies on a specific timescale, to which the former is insensitive. Thus, a second filtered  
 217 estimate  $\hat{\rho}_k^{\tau_{\text{context}}}$  is needed to estimate performance on this timescale. Unlike  $\hat{\rho}_k^{\tau_{\text{long}}}$ , this es-  
 218 timate tracks the effective instantaneous, context-specific performance,  $\rho_{\alpha_k}$ . Its estimation  
 219 error arises from a trade-off, controlled by the integration time,  $\tau_{\text{context}}$ , between its speed  
 220 of adaptation and its finite memory.



221 We consider two distinct hypotheses for how to extend AR-RL to settings where perfor-  
222 mance varies over context. The first hypothesis,  $\mathcal{C}_t^{\text{del}} = \rho_\alpha t$ , is the straightforward, *trial-*  
223 *unaware* extension of eq. (3), shown in fig. 2b(top). Here, performance is tracked only  
224 on a timescale sufficient to capture context variation and the corresponding cost estimate,  
225  $\hat{\rho}_{k-1}^{\text{context}}$ , is incurred moment-to-moment, neglecting the trial-based task structure. However,  
226 this incorrectly lumps together two distinct opportunity costs: those incurred by moment-  
227 by-moment decisions and those incurred as a result of the effective planning implied by  
228 performance that varies over context. In particular, context is defined over trials not mo-  
229 ments, and thus the context-specific component of opportunity cost of a trial is a sunken  
230 cost paid at the outset of a trial. This inspires a second *trial-aware* hypothesis

$$\mathcal{C}_t^{\text{del}} = \rho t + (\rho_\alpha - \rho)T_\alpha. \quad (\text{trial-aware opportunity cost}) \quad (5)$$

231 Equation (5) is plotted over trial time  $t$  in fig. 2b(bottom). Its first term is the AR-RL  
232 contribution from the stationary opportunity cost of moment-to-moment decisions using  
233 the stationary reward rate,  $\rho$  estimated with  $\hat{\rho}_k^{\text{long}}$ . The second, novel term in eq. (5) is a  
234 context-specific trial cost deviation incurred at the beginning of each trial and computed as  
235 the average deviation in opportunity cost accumulated over a trial from that context ( $T_\alpha$   
236 is the average duration of a trial in context  $\alpha$ ). This deviation fills the cost gap made by  
237 using the stationary reward rate  $\rho$  in the moment-to-moment opportunity cost instead of  
238 the context-specific average reward,  $\rho_\alpha$ . This baseline cost derived from the orange time  
239 series in fig. 2a(bottom) vanishes in expectation, as verified through the mixed-context  
240 ensemble average reward (e.g.  $\rho \equiv \sum_\alpha \rho_\alpha T_\alpha / \sum_\alpha T_\alpha$  when the context is distributed evenly  
241 among trials such that  $\sum_\alpha (\rho_\alpha - \rho)T_\alpha = 0$ ). Thus, this opportunity cost reduces to that  
242 used in AR-RL when ignoring context, and suggests a generalization of average-adjusted  
243 value functions to account for non-stationary context. We estimate this baseline cost using  
244  $(\hat{\rho}_{k-1}^{\text{context}} - \hat{\rho}_{k-1}^{\text{long}})T_{k-1}$ , where we have used the sample  $T_{k-1}$  in lieu of the average  $T_\alpha$ . See fig. S1  
245 for a signal filtering diagram that produces this estimate of eq. (5) from reward history. A  
246 main difference between the cost profiles from the two hypotheses is the cost at early times.  
247 Both the behaviour and neural recordings we analyze below seem to favor the second, trial-  
248 aware hypothesis eq. (5). We hereon employ that version in the main text, and show the  
249 results for the trial-unaware hypothesis in fig. S7.

250

## B. Neuroscience application: PGD in the tokens task

251 In this section, we apply the PGD algorithm to the “tokens task” [16]. We first give a  
252 simulated example with periodic context dynamics. We then present an application to a  
253 set of non-human primate experiments in which context variation was non-stationary [19].  
254 For the latter, we used the decision time dynamics over trials to fit a model for each of the  
255 two subjects. We then validated the models by assessing their ability to explain (1) the  
256 concurrently recorded behaviour via their context-specific behavioural strategies and (2) the  
257 neural activity in premotor cortex (PMd) via the temporal profile of the underlying neural  
258 urgency signals.

259 In the tokens task, the subject must guess as to which of two peripheral reaching targets  
260 will receive the majority of tokens that randomly jump, one by one every 200ms, from a  
261 central pool initialized with a fixed number of tokens. Importantly, after the subject reports,  
262 the interval between remaining jumps contracts to once every 150ms (the “slow” condition)

263 or once every 50ms (the “fast” condition), giving the subject the possibility to save time by  
264 taking an early guess. The interval contraction factor,  $1 - \alpha$ , for slow ( $\alpha = 1/4$ ) and fast  
265 ( $\alpha = 3/4$ ) condition is parametrized  $\alpha \in [0, 1]$ , the incentive strength to decide early, which  
266 then serves as the task context.

267 In contrast to the patch leaving task example from Section A, the tokens task has many  
268 within-trial states and the state dynamics is stochastic. With the  $t^{\text{th}}$  jump labelled  $S_t \in$   
269  $\{-1, 1\}$  serving as the state, for the purposes of prediction, the history of states can be  
270 compressed into the tokens difference,  $N_t = \sum_{i=1}^t S_i$ , between the two peripheral targets  
271 with  $N_0 = 0$ . The dynamics of  $N_t$  is an unbiased random walk (see [fig. 3a](#)), with its current  
272 value sufficient to determine the belief of a correct report,  $b_t$  (computed in [Methods](#)). Since  
273 for binary rewards,  $b_t$  is also the expected reward,  $N_t$  is also sufficient for determining the  
274 opportunity cost of commitment,  $\mathcal{C}_t^{\text{com}}$  ([eq. \(2\)](#)). We display this commitment cost dynamics  
275 in [fig. 3b](#). It evolves on a lattice (gray), always starting at 0.5 (for  $p = 1/2$ ) and ending at 0  
276 for all  $p$ . We assume the agent has learned to track this commitment cost. The PGD agent  
277 uses this commitment cost, along with the estimate of the trial-aware deliberation cost, to  
278 determine when to stop deliberating and report its guess.

### 280 1. A simulated example for a regularly alternating context sequence

281 We first show the behaviour of the PGD algorithm in the simple case where  $\alpha$  switches  
282 back and forth every 300 trials (see [fig. 3](#)). We call such segments of constant  $\alpha$  ‘trial blocks’,  
283 with context alternating between slow ( $\alpha = 1/4$ ) and fast ( $\alpha = 3/4$ ) blocks. The decision  
284 space in PGD is a space of opportunity costs, equivalent to the alternative decision space  
285 formulated using beliefs [7]. In particular, one can think of the deliberation cost as the  
286 decision boundary ([fig. 3b](#)). This boundary is dynamic (see [Supplemental video](#)), depending  
287 on performance history via the estimates,  $\hat{\rho}_k^{\tau_{\text{context}}}$  and  $\hat{\rho}_k^{\tau_{\text{long}}}$ , of the context-conditioned and  
288 stationary average reward, respectively. The result of these dynamics is effective context  
289 planning: the PGD algorithm sacrifices accuracy to achieve shorter trial duration in trials  
290 of the fast block, achieving a higher context-conditioned reward rate compared to decisions  
291 in the slow block (*c.f.* the slopes shown in the inset of [fig. S2d](#)). This behaviour can be  
292 understood by analyzing the dynamics of  $\hat{\rho}_k^{\tau_{\text{context}}}$  and  $\hat{\rho}_k^{\tau_{\text{long}}}$ , and their effect on the dynamics  
293 of the decision time ensemble.

294 The two performance estimates behave differently from one another solely because of  
295 their distinct integration times. Ideally, an agent would choose  $\tau_{\text{context}}$  to be large enough  
296 that it serves to average over trial-to-trial fluctuations in a context, but short enough to  
297 not average over context fluctuations. In contrast, the value of  $\tau_{\text{long}}$  would be chosen large  
298 enough to average over context fluctuations. We apply those choices in this simulated  
299 example, with rounded values chosen squarely in the range in which the values inferred  
300 from the behaviour in the following application will lie. As a result of this chosen values,  
301 the context estimate  $\hat{\rho}_k^{\tau_{\text{context}}}$  relaxes relatively quickly after context switches to the context-  
302 conditioned stationary average performance (dashed lines in [fig. 3d](#)), but exhibits stronger  
303 fluctuations as a result. The estimate of the stationary reward,  $\hat{\rho}_k^{\tau_{\text{long}}}$ , on the other hand has  
304 relatively smaller variance. This variance results from the residual zigzag relaxation over the  
305 period of the limit cycle. Given the characteristic block duration,  $T_{\text{block}}$ , we can more more  
306 precise. In particular, when  $T_{\text{block}}$  is much less than  $\tau_{\text{long}}$  ( $T_{\text{block}}/\tau_{\text{long}} \ll 1$ ), the within-block  
307 exponential relaxation is roughly linear. Thus, the average unsigned deviation between  $\hat{\rho}_k^{\tau_{\text{long}}}$   
308 and the actual stationary reward,  $\rho$ , can be approximated using  $1 - \exp[-T_{\text{block}}/\tau_{\text{long}}] \approx$

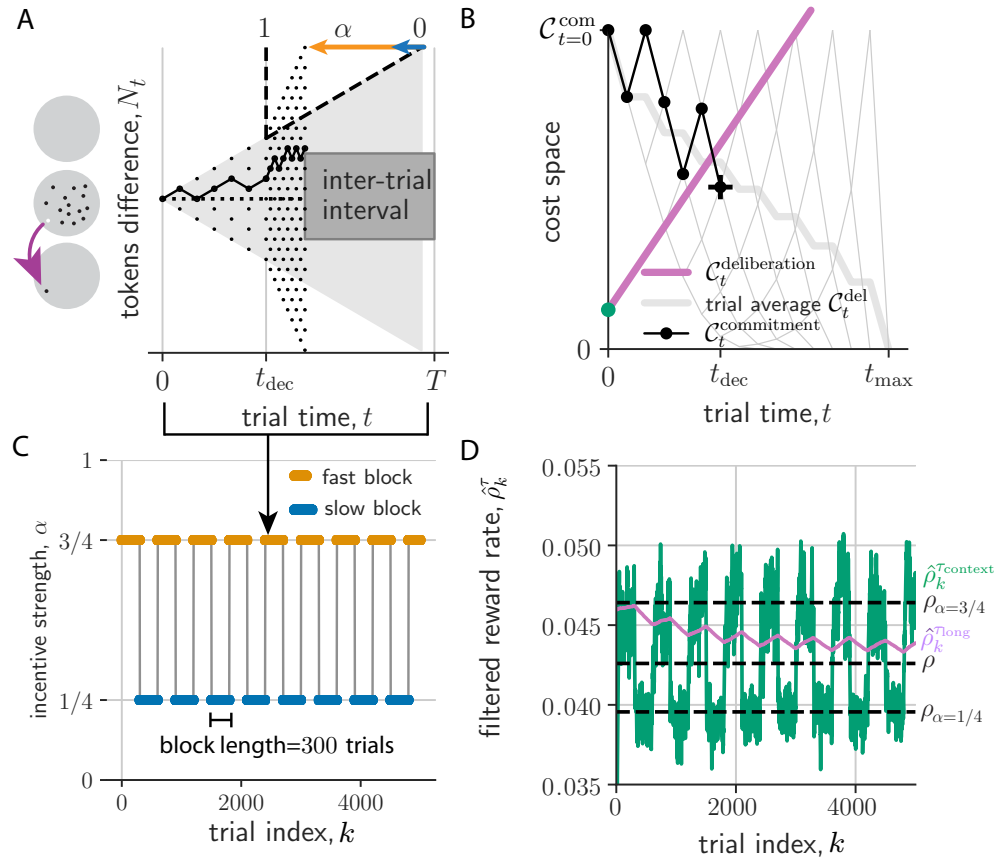


Figure 3. *PGD agent performs the tokens task for periodic context switching.* (a) A tokens task trial. Left: Tokens jump from a center to a peripheral region (gray circles). Right: The tokens difference,  $N_t$ , evolves as a random walk that accelerates according to  $\alpha$  (here  $3/4$ ) post-decision time,  $t^{\text{dec}}$ . The trial duration is  $T$ , which includes an inter-trial interval. (b) Decision dynamics in cost space obtained from evidence dynamics in (a). Commitment cost trajectories (gray lattice; thick gray: trial-averaged) start at  $C_{t=0}^{\text{com}}$  and end at 0. Trajectory from (a) shown in black.  $t^{\text{dec}}$  (black cross) is determined by the crossing of the commitment and deliberation cost. (c) Incentive strength switches between two values every 300 trials. (d) Expected rewards filtered on  $\tau_{\text{long}}$  ( $\hat{\rho}_k^{\tau_{\text{long}}}$ , purple) and  $\tau_{\text{context}}$  ( $\hat{\rho}_k^{\tau_{\text{context}}}$ , green). Black dashed lines from bottom to top are  $\rho_{\alpha=1/4}$ ,  $\rho$ , and  $\rho_{\alpha=3/4}$ .

309  $T_{\text{block}}/\tau_{\text{long}} \ll 1$ . This scaling fits the simulated data well (fig. S2d: inset).

310 The dynamics of these two performance estimates drives the dynamics of the  $k$ -conditioned  
 311 decision time ensemble via how they together determine the deliberation cost (eq. (5); **Sup-**  
 312 **plemental video**). For example, the mean component of this ensemble relaxes after a context  
 313 switch to the context-conditioned average, while the fluctuating component remains strong  
 314 due to the sequence of random walk realizations (fig. S2c). In the case of periodic context,  
 315 the performance estimates and thus also the decision time ensemble relax into a noisy peri-  
 316 odic trajectory over the period of a pair of fast and slow blocks (fig. 3d). Over this period,  
 317 they exhibit some stationary bias and variance relative to their corresponding stationary  
 318 averages (distributions shown in fig. S2e).

319

## 2. *Fit to behavioural data from non-human primates and model validation*

320 Next, we fit a PGD agent to each of the two non-human primates' behaviour in the  
321 tokens task experiments reported in [19]. As with the above example (*c.f.* fig. 3), trials were  
322 structured in alternating blocks of two values of  $\alpha$ . We used the actual context-switching  
323  $\alpha$ -sequence from these experiments, which, in contrast to the above example, exhibits large,  
324 irregular fluctuations in block size, primarily as a result of the experimenter adapting to  
325 fluctuations in motivation of the subject (see fig. 5a)[29].

326 So far, PGD has only two free parameters: the two filtering time constants,  $\tau_{\text{long}}$  and  
327  $\tau_{\text{context}}$ . We anticipated only a weak dependence of the fit on the  $\tau_{\text{long}}$ , so long as it exceeded  
328 the average duration of a handful of trial blocks enabling a sufficiently precise estimate of  
329  $\rho$ . In contrast, the context filtering timescale,  $\tau_{\text{context}}$ , is a crucial parameter as it dictates  
330 where the PGD agent lies on a bias-variance trade-off in estimating  $\rho_{\alpha_k}$ , the value of which  
331 determines the context-specific contribution to the deliberation cost (eq. (2)). To facilitate  
332 the model's ability to fit individual differences, we introduce a subjective reward bias factor,  
333  $K$ , that scales the rewards fed into the performance filters. We also added a tracking-  
334 cost sensitivity parameter,  $\nu$ , that controls  $\tau_{\text{context}}$  to avoid wasting adaptation speed (see  
335 Methods for details). The latter made it possible to fit the asymmetric switching behaviour  
336 observed in the average decision time dynamics. With these four parameters, we could  
337 quantitatively match the average decision time dynamics around the two context switches  
338 (fig. 4a,b; see Methods for fitting details). A comparison of the best-fitting parameter values  
340 over the two monkeys (fig. 4c-e) suggests that the larger the reward bias (fig. 4d), the more  
341 hasty the context-conditioned performance estimate (the smaller  $\hat{\tau}_{\text{context}}$ ), and the lower the  
342 sensitivity to the tracking cost (fig. 4e). This is consistent with the hypothesis that subjects  
343 withhold cognitive effort in contexts of higher perceived reward [8]. Inspecting the shape of  
344 the basins around the best-fitting values, we confirmed our expectation that the fitting error  
345 along the  $\tau_{\text{long}}$  dimension was relatively flat above a soft lower bound (around 5000 time  
346 steps in fig. 4c; the upper bound for visually acceptable fits was imposed by the duration of  
347 the experiment). Indeed, this error basin was much wider in this dimension than along the  
348  $\tau_{\text{context}}$ -dimension. Along with the correspondence in temporal statistics of the behaviour  
349 (e.g. fig. S6), the fitted model parameters for the two subjects provides a basis on which  
350 to interpret the subject differences in the results of the next section, in particular their  
351 separation on a speed-accuracy trade-off, as originating in the distinct reward sensitivity  
353 shown here.

354 With the models fit, we then tested them on the state-dependence of their decisions. A  
355 robust and rich representation of the behavioural statistics is the state and time-conditioned  
356 survival probability that a decision has not yet occurred. It serves as a summary of the  
357 action policy associated with a stationary strategy (see Methods for its calculation from  
358 response times). Applied equally to the decision times of both model and data, it can  
359 provide a means of comparison even in this non-stationary setting. We give this conditional  
360 probability for each of the two contexts for subject 1 in fig. 5b-e. We left the many possible  
361 noise sources underlying the behaviour out of the model in order to more clearly demonstrate  
362 the PGD algorithm. However, such noise sources would be necessary to quantitatively match  
363 the variability in the data (e.g. added noise in the performance estimates leads to larger  
364 variability in the location of the decision boundary and thus also to larger spread in these  
365 survival probability functions (not shown)). In the absence of these noise sources, we see the  
366 model underestimates the spread of probability over time and tokens state. Nevertheless,

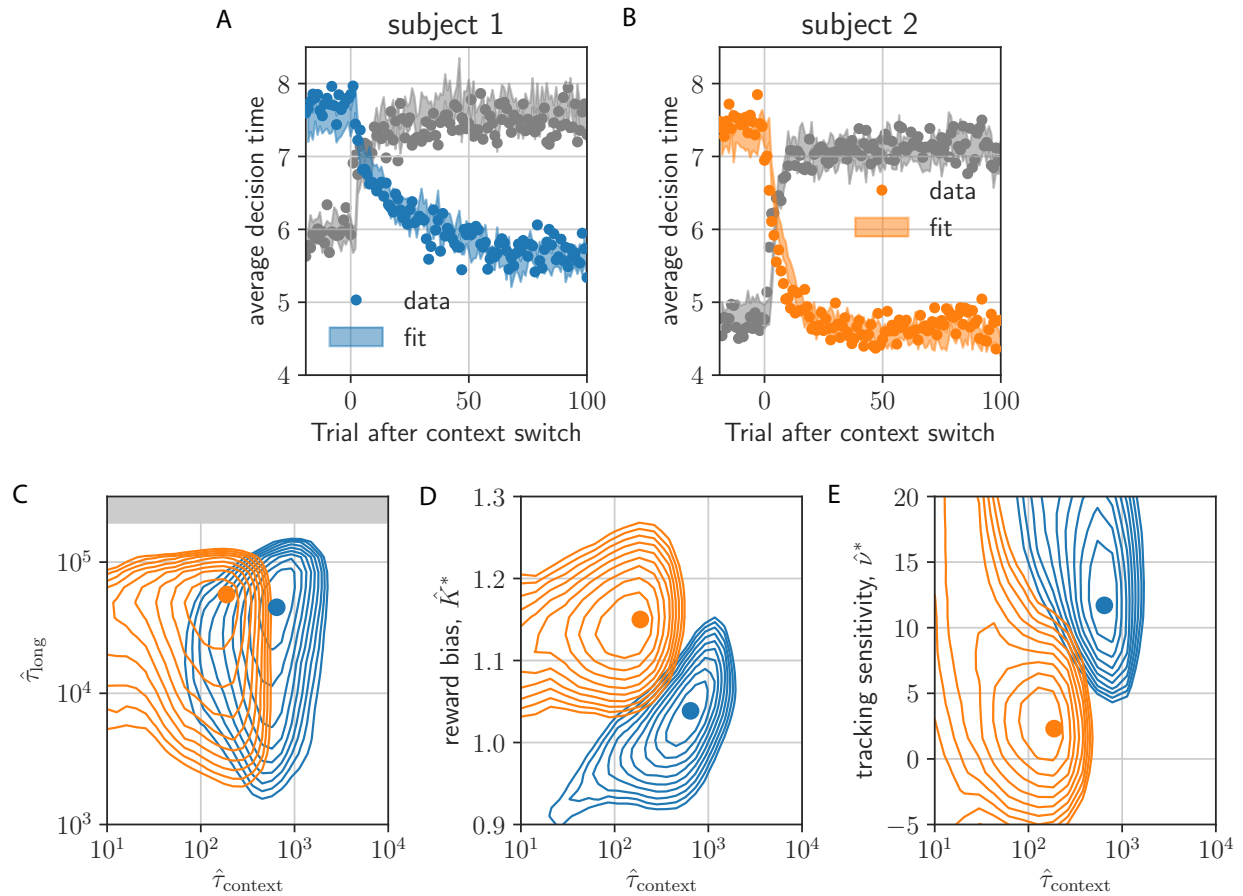


Figure 4. *Model fit.* (a,b) decision times (dots) aligned on the context-switching event type (fast-to-slow in gray; slow-to-fast in color) and averaged. Shaded regions are the standard error bounds of the models' average decision times. (c) Error evaluated on a  $(\hat{\tau}_{\text{context}}, \hat{\tau}_{\text{long}})$ -plane cut through the parameter space at the best-fitting  $\nu = \hat{\nu}^*$  and  $K = \hat{K}^*$  (gray area indicates timescales within an order of magnitude of the end of the experiment). Contours show the first 10 contours incrementing by 0.01 error from the minimum (shown as a circle marker). Colors refer to subject, as in (a) and (b). (d) Same for  $(\hat{\tau}_{\text{context}}, \hat{K})$  at  $\hat{\tau}_{\text{long}} = \hat{\tau}_{\text{long}}^*$  and  $\nu = \hat{\nu}^*$ . (e) Same for  $(\hat{\tau}_{\text{context}}, \hat{\nu})$  at  $\hat{\tau}_{\text{long}} = \hat{\tau}_{\text{long}}^*$  and  $K = \hat{K}^*$ .

367 the remarkably smooth average strategy is well captured by the model (white dashed lines  
 368 in fig. 5c-e). Specifically, policies approximately decide once either of the peripheral targets  
 369 receive a certain number of tokens. Comparing results across context, we find that fast  
 370 block strategies (fig. 5d,e) exhibit earlier decision times relative to slow block strategies  
 371 (fig. 5d,e) in both model and data. The strategies for subject 2 are qualitatively similar,  
 372 but shifted to earlier times relative to subject 1 (fig. S3). Our model explains this subject  
 373 difference as resulting from subject 2's larger reward bias and faster context integration (*c.f.*  
 374 fig. 4d). The correspondence between model and data over the many token states in fig. 5b-e  
 375 is remarkable given that the model has essentially only a single, crucial degree of freedom  
 376 ( $\tau_{\text{context}}$ ), *a priori* unrelated to how decision times depend on token state.

377 To better understand where both the data and the PGD agent lie in the space of strategies  
 378 for the tokens task, we computed reward-rate (AR-RL) optimal solutions for a given fixed



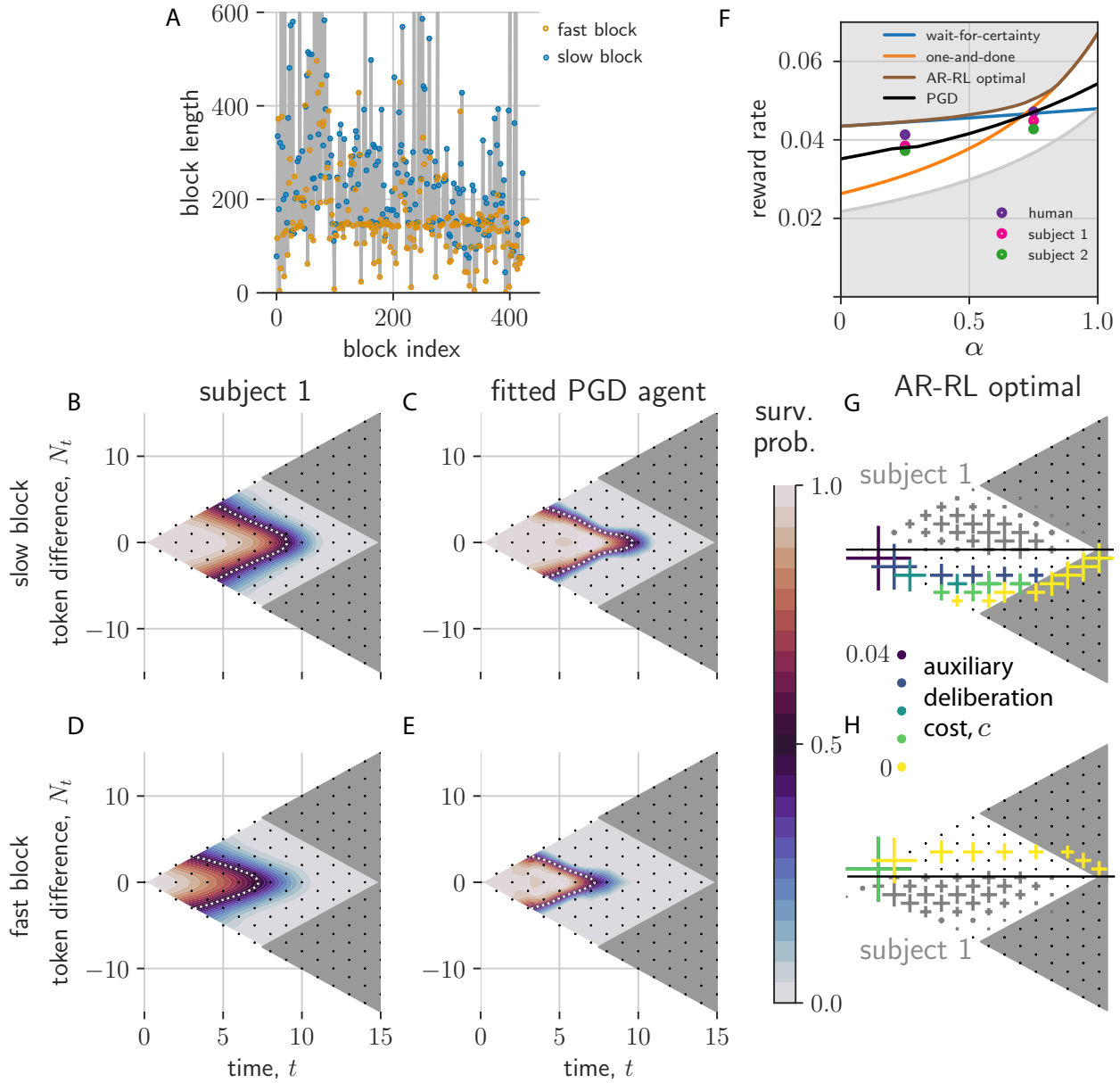


Figure 5. Comparison of PGD to NHP data for non-stationary  $\alpha$ -dynamics from Ref. [19]. (a) Block length sequence used in the experiment (c.f. fig. 3c). (b-e) Interpolated state-conditioned survival probabilities,  $P(t^{\text{dec}} = t | N_t, t)$ , over slow (b,c) and fast (d,e) blocks. White dotted lines show the  $P(t^{\text{dec}} = t | N_t, t) = 0.5$  contour. (f) Shown is the reward rate as a function of incentive strength,  $\alpha$  (wait-for-certainty strategy shown in blue; one-and-done strategy shown in orange). We additionally show the slow and fast context-conditioned reward rates for the two primates as well as a reference expert human, and the PGD solution (black line). Reward rates for the human and non-human primates are squarely in between the best (brown) and uniformly random (gray) strategy. (g,h) State-conditioned decision time frequencies (cross size) from AR-RL optimal decision boundaries across different values of the auxiliary deliberation cost (colored crosses) for slow (g) and fast (h) conditions. Only samples with  $N_t < 0$  and  $N_t > 0$ , respectively, are shown. The reflected axes shows as gray crosses the subject's state-conditioned decision time frequencies for comparison.



379 context,  $\alpha$  (here  $\alpha \in [0, 1]$ ), using the same approach as [7]. Iterating Bellman’s equation  
380 for this decision problem backwards from the end of the trial provides the optimal value  
381 functions from which the optimal policy and its reward rate can be obtained (see [Methods](#) for  
382 details). The optimal reward rate as a function  $\alpha$  is shown in [fig. 5f](#). The optimal strategies  
383 generating these reward rates interpolate from the wait-for-certainty strategy at low  $\alpha$  to  
384 the one-and-done strategy [30] at high  $\alpha$ . The  $\alpha$ -conditioned reward rates achieved by the  
385 two primates and a reference human [31] are also shown in [fig. 5f](#). They fall conspicuously  
386 below the optimal strategy, and, as expected, above the strategy that picks one of the three  
387 actions (report left, report right, and wait) at random. Given the good match in behaviour  
388 between the PGD model and data (*c.f.* [fig. 5b,e](#)), this intermediate performance is shared  
389 by PGD’s solution (black line).

390 What are the differences in decision times that underlie these performance differences?  
391 Both the fitted PGD model and the primate behaviour resolve residual ambiguity ( $N_t \approx 0$ )  
392 at intermediate trial times ([fig. 5b-e](#)). In contrast, the optimal strategies give no intermediate  
393 decision times at ambiguous ( $N_t \approx 0$ ) states, invariably waiting until the ambiguity resolves  
394 (see [fig. 5g,h](#)). To assess the extent of this difference, and for comparison with previous  
395 work [7], we added to the reward objective a constant auxiliary deliberation cost rate,  $c$ ,  
396 incurred up to the decision time in each trial. We find that the resulting optimal strategies  
397 lack intermediate decision times at ambiguous states for all  $c > 0$  and in fact over the entire  
398  $(\alpha, c)$ -plane ( see [fig. S9](#) for the complete dependence). This holds also under the addition of  
399 a movement cost, i.e. a constant cost incurred by either of the reporting actions (data not  
400 shown). Thus, whereas optimal policies shift around the edges of the relevant decision space  
401 as  $\alpha$  or  $c$  is varied, the PGD policy lies squarely in the bulk, tightly overlaying the policy  
402 extracted from the data. We conclude that the context-conditioned strategies of the non-  
403 human primates in this task are well-captured by PGD, while having little resemblance to the  
404 behaviour that would maximize reward rate with or without a fixed auxiliary deliberation  
405 cost rate.

### 406 3. Neural urgency and context-dependent opportunity cost

407 So far, we have fit and analyzed the PGD model with respect to recorded behaviour. Here,  
408 we take a step in the important direction of confronting the above theory of behaviour with  
409 the neural dynamics that we propose drive it. The proposal for the tokens task mentioned  
410 at the end of the introduction has evidence strength and urgency combining in PMd, whose  
411 neural dynamics implements the decision process. In [fig. 6a](#), we restate in a schematic  
412 diagram an implementation of this dynamics that includes a collapsing decision boundary.  
413 In the one-dimensional belief space for the choice ([fig. 6a\(top\)](#)) [7, 32], the rising belief  
414 collides with the collapsing boundary to determine the decision time. In the equivalent  
415 commitment and deliberation cost formulation developed here ([fig. 6a\(middle\)](#)), the falling  
416 commitment cost collides with the rising deliberation cost. The collapsing boundary in  
417 belief space can be parametrized as  $C - u_t$ , where  $C$  is the initial strength of belief, e.g.  
418 some desired confidence, that is lowered by a growing function of trial time  $u_t > 0$ . The  
419 decision criterion is then  $b_t > C - u_t$ , where  $b_t$  is the belief, i.e. the probability of a correct  
420 report. For AR-RL optimal policies,  $u_t$  emerges from value maximization and thus has a  
421 complicated dependence on the opportunity cost sequence,  $\mathcal{C}_t^{\text{del}}$ . For PGD, in contrast,  $C$   
422 is interpreted as the maximum reward  $r_{\text{max}}$  and  $u_t$  is identically  $\mathcal{C}_t^{\text{del}}$ . For a linear neural  
423 encoding model in which belief, rather than evidence, is encoded in neural activity, the sum

424 of the encoded belief  $\tilde{b}_t$  and the encoded collapsing boundary,  $\tilde{u}_t$ , evolve on a one-dimensional  
425 choice manifold. According to the proposal, when this sum becomes sufficiently large (e.g.  
426  $\tilde{b}_t + \tilde{u}_t > \tilde{C}$  for some threshold  $\tilde{C}$ ), PMd begins to drive the activity in downstream motor  
427 areas towards the associated response.

428 Neural urgency was computed from the PMd recordings of [19] in [33]. This computation  
429 relies on the assumption that while a single neuron's contribution to  $\tilde{b}_t$  will depend on  
430 its selectivity for choice (left or right report), the urgency  $\tilde{u}_t$  is a signal arising from a  
431 population-level drive to all PMd neurons, irrespective of their selectivity. Thus,  $\tilde{u}_t$  can  
432 be extracted from neural recordings by conditioning on zero-evidence states ( $\tilde{b}_t = 0$ ) and  
433 averaging over cells. In [33], error bars were computed at odd times via bootstrapping; data  
434 at even times was obtained by interpolating between  $N_t = \pm 1$ ; and data was pooled from  
435 both subjects. We have excluded times at which firing rate error bars exceed the range  
436 containing predictions from both blocks. To assess the correspondence of the components  
437 of the deliberation cost developed here and neural urgency, in fig. 6b we replot their result  
438 (*c.f.* fig.8b of [33]). We overlay the mean (+/- standard deviation) of the opportunity cost  
439 sequence,  $C_t^{\text{del}}$  (shaded area in fig. 4; averaged over all trials produced by applying the two  
440 fitted PGD models on the data sequence and conditioning the resulting average within-  
441 trial deliberation cost on context). To facilitate our qualitative comparison, we convert  
442 cost to spikes/step simply by adjusting the y-axis of the deliberation cost. The observed  
443 urgency signals then lie within the uncertainty of the context-conditioned deliberation cost  
444 signals computed from the fitted PGD models. There are multiple features of the qualitative  
445 correspondence exhibited in fig. 6b: (1) the linear rise in time; (2) the same slope across  
446 both fast and slow conditions; and (3) the baseline offset between conditions, where the fast  
447 condition is offset to higher values than the slow condition. Such features would remain  
448 descriptive in the absence of a theory. With the theory we have presented here, however,  
449 each has their respective explanations via the interpretation of urgency as the opportunity  
450 cost of deliberation: (1) the subject uses a constant cost per token jump, (2) this cost rate  
451 refers to moment-to-moment decisions, irrespective of context, that is reflective of the use  
452 of the context-agnostic stationary reward, and (3) trial-aware planning over contexts leads  
453 to an opportunity cost baseline offset with a sign given by the reward rate deviation  $\rho_\alpha - \rho$   
454 with respect to the stationary average,  $\rho$ .

455 Up to now, the computational and neural basis for urgency has remained largely un-  
456 explored in normative approaches, which also typically say little about adaptation effects  
457 (see [34] for a notable exception). In summary, we exploited the adaptation across context  
458 switches to learn the model and explained earlier responses in high reward rate contexts  
459 as the result of a higher opportunity cost of deliberation. While this qualitative effect is  
460 expected, we go beyond existing work by quantitatively predicting the average dependence  
461 on both time and state (fig. 5b-e) as well as the qualitative form of urgency signal (fig. 6b).  
462 Taken together, the data is thus consistent with our interpretation that neural activity un-  
463 derlying context-conditioned decisions is gated by opportunity costs reflective of a trial-aware  
464 timescale hierarchy computed using performance estimation on multiple timescales.

## DISCUSSION

466 We have proposed PGD, a heuristic decision-making algorithm for continuing tasks that  
467 gates deliberation based on performance. We constructed a foraging example for which

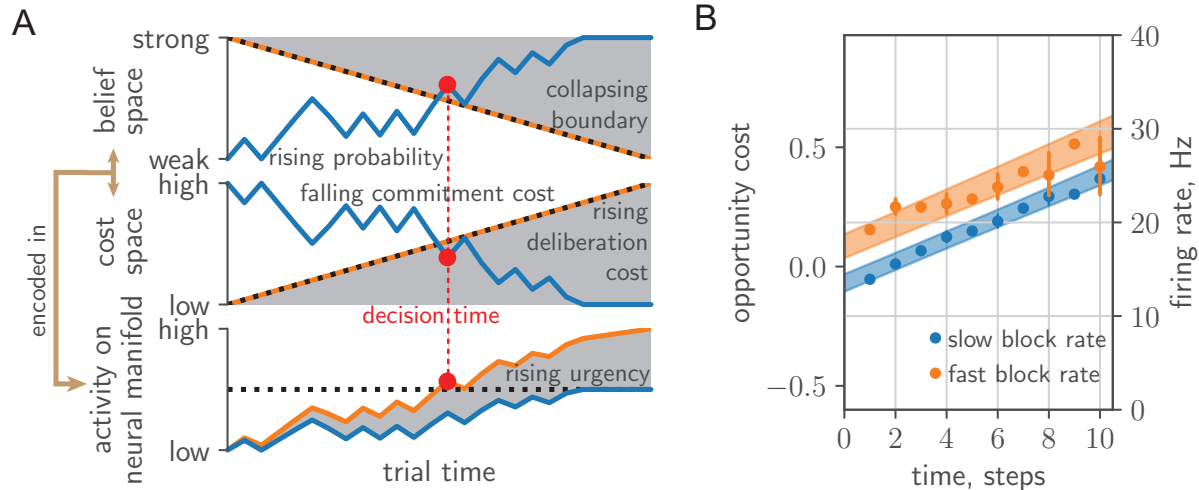


Figure 6. *Comparing neural urgency and collapsing decision boundaries.* (a) Top: Rising belief (blue) meets collapsing decision boundary (black dashed) in belief space. Middle: Falling commitment cost (blue) meets rising deliberation cost (black-dashed) in cost space. Bottom: Belief/commitment cost is encoded (blue) into a low-dimensional neural manifold, with the addition of an urgency signal (orange) (*c.f.* fig.8 in [7]). The decision (red circle) is taken when the sum passes a fixed threshold (black-dashed). (b) Deliberation cost maps onto the urgency signal extracted from zero-evidence conditioned cell-averaged firing rate in PMd.

468 PGD is the optimal strategy with respect to the average-adjusted value function of average-  
 469 reward reinforcement learning (AR-RL). While this will not be true in general, PGD does  
 470 strike a balance between strategy complexity and return. The PGD decision rule does not  
 471 depend on task specifics and exploits the stationarity of the environment statistics while  
 472 simultaneously hedging against longer term non-stationarity in reward context. It does  
 473 so by splitting the problem into two separate components—learning the statistics of the  
 474 environment in order to form the opportunity cost of commitment, and tracking one’s own  
 475 performance in that environment in order to form the opportunity cost of deliberation.  
 476 Within our current understanding of how the cortico-basal ganglia system supports higher-  
 477 level decision-making [35], this latter cost is proposed as arising from performance estimated  
 478 on multiple, behaviourally-relevant timescales that are broadcast to multiple, lower-level  
 479 decision-making areas to gate the speed of their respective attractor-based decision-making  
 480 dynamics (models of the latter are well-studied [32, 36, 37]). Consistent with this picture,  
 481 PGD’s explanatory power was borne out at both the behavioural and neural levels for the  
 482 tokens task data we analyzed. In particular, a deliberation cost constructed from trial-aware  
 483 planning was supported independently by both modalities. We used behavioural data to  
 484 fit and validate the theory, and neural recordings to provide evidence of one of the neural  
 485 correlates it proposes: the temporal profile of neural urgency.

486 *Scientific and clinical implications* In our proposal, we have linked two important and  
 487 related, but often disconnected fields: the systems neuroscience of the neural dynamics of  
 488 decision-making and the cognitive neuroscience of opportunity cost and reward sensitivity.  
 489 The view that tonic dopamine encodes average reward is two decades old [3]. However,  
 490 the existence of a reward representation decomposed by timescale has received increasing  
 491 empirical support in recent years, from cognitive results [38–40] to a recent unified view of

492 how dopamine encodes reward prediction errors using multiple discount factors [41, 42] and  
493 of dopamine as encoding both value and uncertainty [43]. Dopamine’s effect on time per-  
494 ception has been proposed [44] and has empirical support [45], but the mechanism by which  
495 its putative effect on decision speed is implicated in the neural dynamics of the decision-  
496 making areas driving motor responses was unknown. Our theory fills this explanatory gap  
497 by considering dynamic evidence tasks and parametrizing urgency using a multiple-timescale  
498 representation of performance. One candidate for the latter’s neural implementation is in the  
499 complex spatio-temporal filtering of dopamine via release-driven tissue diffusion and integra-  
500 tion via DR1 and DR2 binding kinetics [46]. Subsequent neural filtering and computation  
501 by striatal network activity could also play a role [47]. The study of spatiotemporal filtering  
502 of dopamine is increasingly accessible experimentally [48, 49] and provides an exciting direc-  
503 tion for multi-scale analysis of behaviour. Our proposal that urgency is the means by which  
504 the neural representation of reward ultimately affects neural dynamics in decision-making  
505 areas frames a timely research question on which these questions could shed light.

506 While we applied PGD to decisions playing out in PMd, a decision-making area relevant  
507 to arm movements, PGD may also be relevant to other kinds of decisions. For instance,  
508 a large body of work has studied decisions playing out in lateral intraparietal cortex using  
509 random dot motions tasks. One seminal study identified an urgency signal with the same  
510 properties: a linear dependence at early trial times and an offset with sign given by the  
511 reward rate deviation across two and four-choice trials, which serve as the two contexts [17].  
512 In contrast to the tokens task, however, context was sampled randomly and thus its dynamics  
513 lacked temporal correlation. In this case, we might expect that a pair of performance filters,  
514 one for each context, to track the reward history in two parallel streams, each updated only  
515 when in their respective context. In this case, our theory would predict that the ratio of  
516 slopes of urgency reflect the ratio of context-conditioned reward rates. An estimation given  
517 in the [Methods](#) for this data [17] agrees to within 20% error, providing preliminary support  
518 for our theory. Testing the generality of our theory using tailored experiments in this other  
519 setting is an important next step.

520 Urgency may play a role in both decision and action processes, potentially providing a  
521 transdiagnostic indicator of a wide range of cognitive and motor impairments in Parkinson’s  
522 disease and depression [50]. Our theory offers a means to ground these diverse results in  
523 neural dynamics by formulating opportunity cost estimation as the underlying causal factor  
524 linking vigor impairments (e.g. in Parkinson’s disease) and dysregulated dopamine signalling  
525 in the reward system [50–52]. We provide a concrete proposal for a signal filtering system  
526 that extracts a context-sensitive opportunity cost from a reward prediction error sequence  
527 putatively encoded by dopamine. Neural recordings of basal ganglia provide a means to  
528 identify the neural substrate for this system.

529 *Commitment cost estimation* Beyond the estimation of the opportunity cost of deliber-  
530 ation, we assumed that the agent had a precise estimate of the expected reward, which it  
531 used to compute the within-trial commitment cost. For the tokens task, a recorded signal in  
532 dorsal lateral prefrontal cortex of non-human primates correlates strongly with belief [20],  
533 equivalent to the expected reward for binary rewards). How this quantity is computed by  
534 neural systems is not currently known. However, for a general class of tasks, a generic,  
535 neurally plausible means to learn the expected reward is via distributional value codes [43].  
536 For example, the Laplace code is a distributional value representation that uses an ensemble  
537 of units over a range of temporal discount factors and reward sensitivities [53]. The authors  
538 show that expected reward is linearly decodeable from this representation.

539 *Experimental predictions* A feature of our decision-making theory is that it is highly  
540 vulnerable to falsification. First, with regards to behaviour via the shape of the action  
541 policy using our survival probability representation (*c.f.* fig. 5b-e,g,h), PGD varies markedly  
542 with reward structure and thus provides a wealth of predictions for how observed behaviour  
543 should be altered by it. For example, a salient feature of the standard tokens task is its  
544 reflection symmetry in the tokens difference,  $N_t$ . We can break this symmetry for which the  
545 theory predicts a distinctly asymmetric shape (fig. S10; for details see [Methods](#)). Our theory  
546 is also prescriptive for neural activity via the temporal profile of neural urgency. The slope of  
547  $C_t^{\text{del}}$  remained fixed across blocks for relatively short block lengths used in the data analyzed  
548 here. In the opposite limit,  $T_{\text{block}}/\tau_{\text{long}} \gg 1$ ,  $\rho_k^{\tau_{\text{long}}}$  approaches  $\rho_\alpha$  except when undergoing  
549 large, transient excursions after context switches. Thus, the deliberation cost is given by  
550 the first component in eq. (5) most of the time, with the context specific reward rate as the  
551 slope. One simple prediction is that the slope of urgency should exhibit increasing variation  
552 as the duration of the blocks increases.

553 *Reinforcement learning theory* Our work impacts reinforcement learning theory by sug-  
554 gesting how to generalize average-adjusted value functions to time-varying opportunity cost  
555 of time in a way that reduces to AR-RL when context is not tracked. This further develops  
556 episodic AR-RL in the continuing task setting, which has received relatively little attention  
557 from AR-RL machine learning research, and yet is central to experimental neuroscience.  
558 The epistemic perspective entailed in the estimation of these costs parallels a recent epis-  
559 temic interpretation of the discount-reward formulation as encoding knowledge about the  
560 volatility of the environment [54].

561 Our work also suggests a new class of reinforcement learning algorithms between model-  
562 based and model-free: only parts of the algorithm need adjustment upon task structure  
563 variation. This is reminiscent of how the effects of complex state dynamics are decoupled  
564 from reward when using a successor representation [55], but tailored for the average-reward  
565 rather than the discount-reward formulation. We have left a detailed algorithmic analysis of  
566 PGD to future work, but expect performance improvements, as with successor representa-  
567 tions, in settings where decoupling the learning of environment statistics from the learning  
568 of reward structure is beneficial.

569 *Comparison with humans* In the space of strategies, PGD lies in a regime between fully  
570 exploiting assumed task knowledge (average-case optimal) and assumption-free adaptation  
571 (worst-case optimal). Highly incentivized human behaviour is likely to be more structured  
572 than PGD because of access to more sophisticated learning. While some humans land on  
573 the optimal one-and-done policy in the fast condition when playing the tokens task [56],  
574 most do not. The human brain likely has all the components needed to implement PGD.  
575 Nevertheless, the situations in which we actually exploit PGD, if any, are as yet unclear. In  
576 particular, how PGD and AR-RL relate to existing behavioural models tailored to explain  
577 relative-value, context-dependent decision-making in humans [4], such as scale and shift  
578 adaptation[57], is an open question. Whether or not PGD is built into our decision-making,  
579 the question remains if PGD is optimal with respect to some bounded rational objective.  
580 In spite of the many issues with the latter approach [58], using it to further understand the  
581 computational advantages of PGD is an interesting direction for future work.

582 Despite our putative access to sophisticated computation, humans still exhibit measurable  
583 bias in how we incorporate past experience [59]. One simple example is the win-stay/lose-  
584 shift strategy, a more rudimentary kind of performance-gated decision-making than PGD,  
585 which explains how humans approach the rock-paper-scissors game [60]. In that work,



586 numerical experiments demonstrated that this strategy outperforms at a population level the  
587 optimal Nash equilibrium for this game, demonstrating that the use of such seemingly sub-  
588 optimal strategies can confer a surprising evolutionary advantage. This example supports  
589 the claim that relatively simple and nimble strategies such as PGD make for attractive  
590 candidates when acknowledging that a combination of knowledge and resource limitations  
591 over task, development, and evolutionary timescales have shaped decision-making in non-  
592 stationary environments.

593

## METHODS

594 Code for simulations and main figure generation (written in Python 3) is publicly acces-  
595 sible as a online repository: [https://github.com/mptouzel/dyn\\_opp\\_cost/](https://github.com/mptouzel/dyn_opp_cost/).

596

### Patch leaving task

597 We devised a mathematically tractable patch leaving task for which PGD learning is  
598 optimal with respect to the average-adjusted value function. Here the value is simply the  
599 return from the patch. This value function is related, but not equivalent to the marginal  
600 value of optimal foraging, for which the decision rule is  $C_t^{\text{del}} > r_{\text{max}} - C_t^{\text{com}} = \bar{r}_t$  [5]. This  
601 choice of task allowed us to compare PGD’s convergence properties relative to conventional  
602 AR-RL algorithms that make use of value functions. In contrast to PGD, the latter requires  
603 exploration. For a comparison generous to the AR-RL algorithm, we allowed it to circumvent  
604 exploration by estimating the value function from off-policy decisions obtained from the  
605 PGD algorithm using the same learning rate. We then compared them to PGD using their  
606 on-policy, patched-averaged reward. This made for a comparison based solely between the  
607 parameters of the respective models. If we did not allow for this, the  
608 ar-RL algorithms would have to find good learning signals by exploring. In any form, this  
609 exploration would lead them converge substantially slower. This setting thus provides a  
610 lower bound on the convergence times of the AR-RL algorithm.

611 In this task, the subject randomly samples (with replacement)  $d$  patches, each of a dis-  
612 tinct, fixed, and renewable richness defined by the maximum return conferred. These maxi-  
613 mum returns are sampled before the task from a richness distribution,  $p(r_{\text{max}})$ , with  $r_{\text{max}} > 0$   
614 and are fixed throughout the experiment. The trials of the task are temporally extended  
615 periods during which the subject consumes the current patch. After a time  $t$  in a patch,  
616 the return is defined  $r(t) = r_{\text{max}}(1 - (\lambda t)^{-1})$ . This patch return profile,  $1 - (\lambda t)^{-1}$ , is shared  
617 across all patches and saturates in time with rate  $\lambda$ , a parameter of the environment that  
618 sets the reference timescale. The return diverges negatively for vanishing patch leaving times  
619 for mathematical convenience, but also evokes situations where leaving a patch soon after  
620 arriving is prohibitively costly (e.g. when transit times are long). A stationary policy is then  
621 a leaving time,  $t_s$ , for each of  $d$  patches, where the  $s$ -subscript indexes the patch. Given any  
622 policy, the stationary reward rate for uniformly random sampling of patches is then defined  
623 as

$$\rho = \frac{\sum_{s=1}^d r_s(t_s)}{\sum_{s=1}^d t_s} . \quad (6)$$

624 We designed this task to (1) emphasize the speed-return trade-off typical in many delibera-



tion tasks, and (2) have a tractable solution with which to compare convergence properties of PGD and AR-RL value function learning algorithms.

A natural optimal policy is the one that maximizes the average-adjusted trial return,  $Q(r, t) = r - \rho t$ . Given the return profile we have chosen, the corresponding optimal decision time,  $t_s^*$ , in the  $s$ th patch obtained by maximizing  $r - \rho t$  is  $t_s^* = \sqrt{r_{\max, s} / (\lambda \rho)}$ , which scales inversely with the reward rate so that decision times are earlier for larger reward rates, because consumption (or more generally deliberation) at larger reward rates costs more. We chose this return profile such that stationary PGD learning gives exactly the same decision times: the condition  $\mathcal{C}_t^{\text{del}} = \mathcal{C}_t^{\text{com}}$  for patch  $s$  here takes the form  $\rho t_s = r_{\max, s} / (\lambda t_s)$ . Thus, they share the same optimal reward rate,  $\rho^*$ . Using  $t_s^*$  for each patch in eq. (6) gives a self-consistency equation for  $\rho$  with solution  $\rho^* = \lambda \mu_1^2 / 4 \mu_{1/2}^2$ , where  $\mu_n = \langle r_{\max}^n \rangle_{p(r_{\max})}$  (we have assumed  $d$  is large here to remove dependence on  $s$ ). Described so far in continuous time, the value function was implemented in discrete time such that the action space is a finite set of decision times selected using the greedy policy,  $t^* = \operatorname{argmax}_t \hat{Q}(r, t)$ , where  $\hat{Q}(r, t)$  is the estimated trial return. As a result, there is a finite lower bound on the performance gap, i.e. the relative error,  $\epsilon = (\rho^* - \rho) / \rho^* > 0$  for the AR-RL algorithm. Approaching this bound, convergence time for both PGD and AR-RL learning is limited by the integration time  $\tau$  of the estimate  $\hat{\rho}_k^\tau$  (c.f. eq. (8)) of  $\rho$ . We note that PGD learns faster in all parameter combinations tested. To demonstrate the insensitivity of PGD to the state space representation, at  $5 \times 10^5$  time steps into the experiment we shuffled the labels of the states. PGD is unaffected, while the value function-based AR-RL algorithm is forced to relearn and in fact does so slower than in the initial learning phase, due to the much larger distance between two random samples, than between the initial values (chosen near the mean) and the target sample.

649

### Filtering performance history

For unit steps of discrete time, the step-wise update of the performance estimate,  $\hat{\rho}_t^\tau$ , is

$$\hat{\rho}_t^\tau = (1 - \beta) \hat{\rho}_{t-1}^\tau + \beta R_t, \quad (7)$$

with  $\beta = 1 / (1 + \tau)$  called the learning rate, and  $\tau$  the characteristic width of the exponential window of the corresponding continuous time filter over which the history is averaged. We add  $\tau$  as a superscript when denoting the estimate to indicate this. Exceptionally, here  $t$  indexes absolute time rather than trial time. Note that a continuous-time formulation of the update is possible via an event-based map given the decision times in which the reward event sequence is given as a sum of delta functions. In either case, to leading order in  $\beta$ ,  $\hat{\rho}_t^\tau \approx \beta \sum_i^t R_i$ , i.e. the filter sums past rewards. Thus, when  $\tau \sim \mathcal{O}(t) \gg 1$ ,  $\beta \sim \mathcal{O}(1/t) \ll 1$  and so  $\hat{\rho}_t^\tau \approx \beta \sum_i^t R_i \rightarrow \rho$  when  $t$  is large.

The rewards in this task are sparse:  $R_t = 0$  except when a trial ends and the binary trial reward  $R_k$  (1 or 0) is received. A cumulative update of eq. (7) that smooths the reward uniformly over the trial duration and is applied once at the end of each trial is thus more computationally efficient. Resolving a geometric series leads to the cumulative update [8, 28]

$$\hat{\rho}_k^\tau = (1 - \beta)^{T_k} \hat{\rho}_{k-1}^\tau + (1 - (1 - \beta)^{T_k}) \rho_k^{\text{trial}}, \quad (8)$$

where the smoothed reward,  $\rho_k^{\text{trial}} = R_k / T_k$ , can be interpreted as a trial-specific reward rate. The initial estimate,  $\hat{\rho}_0^\tau$ , is set to 0. Exceptionally,  $\hat{\rho}_1^\tau = R_1 / T_1$ , after which eq. (8) is used.

665

666 Using the first finite sample as the first finite estimate is both more natural and robust than  
667 having to adapt from zero. We will reuse this filter for different  $\tau$  and denote the filtered  
668 estimate from its application with a  $\tau$ -superscript,  $\hat{\rho}_k^\tau$ . For example, the precision of  $\hat{\rho}_k^{\tau_{\text{long}}}$   
669 as an estimate of a stationary reward rate  $\rho$  is set by how many samples it averages over,  
670 which is determined by the effective length of its memory given by  $\tau_{\text{long}}$ . Since we assume  
671 the subject has learned the expected reward,  $\bar{r}_t$ , we use it instead of  $R_k$  when computing  
672  $\rho_k^{\text{trial}}$ .

673

### Tokens task: a random walk formulation

674 The tokens task is a continuing task of episodes (here trials), which can be formulated  
675 using the token difference,  $N_t$ . Each trial effectively presents to the agent a realization  
676 of a finite-length, unbiased random walk,  $\mathbf{N}_{t_{\text{max}}} = (N_0, \dots, N_{t_{\text{max}}})$  with  $N_t = \{-t, \dots, t\}$   
677 and  $N_0 = 0$ . We express time in units of these steps. The agent observes the walk and  
678 reports its prediction of the sign of the final state,  $\text{sign}(N_{t_{\text{max}}}) = \pm 1$  ( $t_{\text{max}}$  is odd to exclude  
679 the case it has no sign). The time at which the agent reports is called the decision time,  
680  $t^{\text{dec}} \in \{0, 1, \dots, t_{\text{max}}\}$ . For a greedy policy,  $\text{sign}(N_t)$  can be used as the prediction (and  
681 the reporting action selected randomly if  $N_{t^{\text{dec}}} = 0$ ). The decision-making task then only  
682 involves choosing when to decide. In this case, the subject receives reward  $R = \Theta(N_{t_{\text{max}}} N_{t^{\text{dec}}})$   
683 at the end of the random walk, i.e. a unit reward for a correct prediction, otherwise nothing  
684 ( $\Theta$  is the Heaviside function:  $\Theta(x) = 1$  if  $x > 0$ , zero otherwise).

685 An explicit action space beyond decision time is not necessary for the case of greedy  
686 actions. It can nevertheless be specified for illustration in an Markov decision process (MDP)  
687 formulation: the agent waits ( $a_t = 0$  for  $t < t^{\text{dec}}$ ) until it reports its prediction,  $a_{t^{\text{dec}}} = \pm$ ,  
688 after which actions are disabled and the prediction is stored in an auxiliary state variable  
689 used to determine the reward at the end of the trial. A MDP formulation for a general class  
690 of perceptual decision-making tasks, including the tokens and random dots task, is given in  
691 [Methods](#)).

692 Perfect accuracy in this task is possible if the agent reports at  $t_{\text{max}}$  since  $R = \Theta(N_{t_{\text{max}}}^2) =$   
693 1. The task was designed to study reward rate maximizing policies. In particular, the task  
694 has additional structure that allows for controlling what this optimal policy is through the  
695 incentive to decide early,  $\alpha$ , incorporated into the trial duration for deciding at time  $t$  in the  
696 trial,

$$T(t) = t + (1 - \alpha)(t_{\text{max}} - t) + T_{\text{ITI}}. \quad (9)$$

697 Here, a dead time between episodes is added via the inter-trial interval,  $T_{\text{ITI}}$ , to make  
698 suboptimal the strategy of predicting randomly at the trial's beginning. We emphasize that  
699 it is through the trial duration that  $\alpha$  serves as a task parameter controlling the strength  
700 of the incentive to decide early. When  $\alpha$  is fixed, we denote the corresponding optimal  
701 stationary reward rate,  $\rho_\alpha$ , obtained from the reward rate maximizing policy. This policy  
702 shifts from deciding late to deciding early as  $\alpha$  is varied from 0 to 1 (*c.f.* [fig. S9f,g](#)).

703 We consider a version of the task where  $\alpha$  is variable across two episode types, a slow  
704 ( $\alpha = 1/4$ ) and fast ( $\alpha = 3/4$ ) type. The agent is aware that the across-trial  $\alpha$  dynamics  
705 are responsive (maybe even adversarial), whereas the within-trial random walk dynamics  
706 (controlled by the positive jump probability, here  $p = 1/2$ ) can be assumed fixed (see the  
707 next section for how  $p$  factors into the expression for the expected reward,  $\bar{r}_t$ ).

708

### Expected trial reward for the tokens task

709 We derived and used an exact expression for the expected reward in a trial of the tokens  
 710 task. We derive that expression here as well as a simple approximation. The state sequence  
 711 is formulated as a  $t_{\max}$ -length sequence of random binary variables,  $\mathbf{S}_{t_{\max}} = (S_1, \dots, S_{t_{\max}})$ ,  
 712  $S_t = \pm 1$ ,  $i = 1, 2, \dots, t_{\max}$ . Consider a simple case in which each is an independent and  
 713 identically distributed Bernoulli sample,  $P(s) = p^{\frac{1+s}{2}}(1-p)^{\frac{1-s}{2}}$ , for jump probability  $p \geq 1/2$ .  
 714 The distribution of  $\mathbf{S}_{t_{\max}}$  is then

$$P(\mathbf{s}_{t_{\max}}) = \prod_{i=1}^{t_{\max}} P(s_i). \quad (10)$$

715 We will use this distribution to compute expectations of quantities over this space of trajec-  
 716 tories, namely the sign of  $N_t = \sum_{i=1}^t S_i$ , for some  $0 \leq t \leq t_{\max}$  and in particular the sign of  
 717 the final state,  $\xi := \text{sgn}(N_{t_{\max}}) \in \{+, -\}$  given  $N_t = n$ . Note that  $N_t$  is even if  $t$  is even and  
 718 same with odd values. We remove the case of no sign in  $N_{t_{\max}}$  by choosing  $t_{\max}$  to be odd.

719 First, consider predicting  $\text{sgn}(N_t)$  with no prior information. The token difference,  $-t \leq$   
 720  $N_t \leq t$ , appears directly in  $P(\mathbf{s}_{t_{\max}})$ . Marginalizing (here just integrating out) the additional  
 721 degrees of freedom leads to a binomial distribution in the number of  $S_i$  for  $i \leq t$  for which  
 722  $S_i = +1$ ,  $N_t^+ = \sum_{i=1}^t \Theta(s_i) = (t + N_t)/2$ ,

$$P(N_t^+ = n) = \binom{t}{n} p^n (1-p)^{t-n}, \quad (11)$$

723 with  $n \in \{0, \dots, t\}$  and  $N_t = 2N_t^+ - t$ . Thus, the probability that  $N_t > 0$ , i.e.  $N_t^+ > t/2$ , is

$$P(N_t > 0) = \sum_{n=0}^t \binom{t}{n} p^n (1-p)^{t-n} \Theta(n - t/2). \quad (12)$$

724 Now consider predicting  $\xi = \text{sgn}(N_{t_{\max}})$ , given the observation  $N_t = n$ . Define  $t' = t_{\max} - t$   
 725 as the remaining time steps to the predicted time and  $N_{t'} = \sum_{i=t+1}^{t_{\max}} s_i$ , i.e. the total count  
 726 in the remaining part of the realization. Then the probability of  $\xi = +$  conditioned on the  
 727 state  $N_t = n$ , denoted  $p_{n,t}$ , is defined in the same way as  $P(N_t > 0)$ ,

$$p_{n,t}^+ := P(\xi = + | N_t = n) = \sum_{n'=0}^{t'} \binom{t'}{n'} p^{n'} (1-p)^{t'-n'} \Theta(n' - (t' - n)/2). \quad (13)$$

728 where  $N_{t'}^+ = n'$  is the number of positive jumps in the remaining  $t' = t_{\max} - t$  steps and we  
 729 have used  $N_{t_{\max}} = N_t + N_{t'} = N_{t'}^+ - (t' - N_t)/2$ . The  $\Theta(n' - (t' - n)/2)$  factor effectively changes  
 730 the lower bound of the sum to  $\max\{0, \lceil (t' - n)/2 \rceil\}$ , where  $\lceil \cdot \rceil$  rounds up. If  $\lceil (t' - n)/2 \rceil \leq 0$   
 731 then  $p_{n,t}^+ = 1$  since the sum is over the domain of the distribution, which is normalized.  
 732 Otherwise, the lower bound is  $\lceil (t' - n)/2 \rceil$ , and the probability of  $\xi = +1$  is

$$p_{n,t}^+ = \sum_{n'=\lceil (t'-n)/2 \rceil}^{t'} \binom{t'}{n'} p^{n'} (1-p)^{t'-n'}. \quad (14)$$

733 For odd  $t_{\max}$ , the probability that  $\xi = -$  is denoted  $p_{n,t}^- = 1 - p_{n,t}^+$ . For the symmetric case,  
734  $p = 1/2$ ,

$$p_{n,t}^+ = \frac{1}{2^{t'}} \sum_{n'=\lceil(t'-n)/2\rceil}^{t'} \binom{t'}{n'}, \quad (15)$$

735 when  $\lceil(t' - n)/2\rceil > 0$  and 1 otherwise. This expression is equivalent to equation 5 in [16],  
736 which was instead expressed using  $N_{t'}^-$ .

737 The space of trajectories, i.e. of  $\mathbf{s}_{t_{\max}}$ , maps to a space of trajectories for  $p_{n,t}^+$  defined on  
738 an evolving lattice in belief space. The expected reward in this case is,

$$\bar{r}_t := \langle r | N_t = n \rangle = \mathbb{E}[\Theta(N_{t_{\max}} N_t) | N_t = n] \quad (16)$$

$$= \max\{p_{n,t}^+, 1 - p_{n,t}^+\} \quad (17)$$

$$= b_t, \quad (18)$$

739 where the belief of correct report  $b_t := \max\{p_{n,t}^+, 1 - p_{n,t}^+\}$ . The commitment cost  $\mathcal{C}_t^{\text{com}} =$   
740  $r_{\max} - \bar{r}_t$ , then also evolves on a lattice (see fig. 3(b)). More generally,  $\bar{r}_t = \Delta r b_t + r_{\text{incorrect}}$   
741 for  $\Delta r$  the difference of correct  $r_{\text{correct}}$  (here 1) and incorrect  $r_{\text{incorrect}}$  (here 0) rewards. Since  
742  $r_{\max} = r_{\text{correct}}$ , we have  $\mathcal{C}_t^{\text{com}} = \Delta r(1 - b_t)$ . For  $p = 1/2$  and  $\Delta r = 1$ ,  $\mathcal{C}_{t=0}^{\text{com}} = 1/2$ .

743 The shape of  $p_{n,t}^+$  is roughly sigmoidal, admitting the approximation,

$$p_{n,t}^+ \approx \frac{1}{1 + \exp[-(at + b)n]} \quad (19)$$

744 where fitting constants  $a$  and  $b$  depend on  $t_{\max}$ . For  $t_{\max} = 15$ ,  $a = 0.03725$  and  $b = 0.3557$ .  
745 We demonstrate the quality of this approximation in fig. S5. Approximation error is worse  
746 at  $t$  near  $t_{\max}$ . More than 95% of decisions times in the data we analyzed occur before  
747 12 time steps, where the approximation error in probability is less than 0.05. A similar  
748 approximation without time dependence was presented in [16]. We nevertheless used the  
749 exact expression eq. (15) in all calculations.

## 750 PGD implementation and fitting to relaxation after context switches

751 We identified the times of the context switches in the data and their type (slow-to-fast  
752 and fast-to-slow). Taking a fixed number of trials before and after each event, we averaged  
753 the decision times over the events to create two sequences of average decision times around  
754 context switches (the result is shown in fig. 4a,b). We used a uniformly weighted squared-  
755 error objective, minimized with the standard (Nelder-Mead) simplex routine in python's  
756 scientific computing library's optimization package.

## 757 Survival probabilities over the action policy

758 Behavioural analyses typically focus on response time distributions. From the perspective  
759 of reinforcement learning, this is insufficient to fully characterize the behaviour of an agent.  
760 Instead, the full behaviour is given by the action policy. In this setting, a natural represen-  
761 tation of the policy is the probability to report as a function of both the decision time *and*  
762 the environmental state (see fig. 5). These are computed from the histograms of  $(N_{t^{\text{dec}}}, t^{\text{dec}})$ ,

763 over trials. However, the histograms themselves do not reflect the preference of the agent  
764 to decide at a particular state and time because they are biased by the different frequencies  
765 with which the set of trajectories visit each state and time combination. While there are  
766 obviously the same number of trajectories at early and late times, they distribute over many  
767 more states at later times and so each state at later times is visited less on average than states  
768 at earlier times. We can remove this bias by transforming the data ensemble to the ensemble  
769 of two random variables: the state conditioned on time ( $N_t|t$ ), and the event that  $t = t^{\text{dec}}$ .  
770 Conditioning this ensemble on the state gives  $P(t = t^{\text{dec}}|N_t, t) = p(N_t, t = t^{\text{dec}}|t)/p(N_t|t)$ . To  
771 reduce estimator variance, we focus on the corresponding survival function,  $P(t < t^{\text{dec}}|N_t, t)$ .  
772 So,  $P(t < t^{\text{dec}}|N_t, t) = 1$  when  $t = 0$  and decays to 0 as  $t$  and  $|N_t|$  increase. Unlike the  
773 unconditioned histograms, these survival probabilities vary much more smoothly over state  
774 and time. This justifies the use of the interpolated representations displayed in [fig. 5b-e](#).  
775 Note that to simplify the analysis, we have binned decision times by the 200 ms time step  
776 between token jumps. This is justified by the small deviations from uniformity of decision  
777 times modulo the time step shown in [fig. S11](#).

## 778 Episodic decision-making and dynamic programming solutions of value iteration

779 We generalize the mathematical notation and description of an existing AR-RL formu-  
780 lation and dynamic programming solution of the random dots task [7], a binary perceptual  
781 evidence accumulation task extensively studied in neuroscience. To align notation with  
782 convention in reinforcement learning theory, exceptionally here  $s$  denotes the belief state  
783 variable, ie. a representation of the task state sufficient to make the decision (e.g. the to-  
784 kens difference,  $N_t$ , in the case of the tokens task). We connect this extended formulation to  
785 account for a dynamic deliberation cost. We write it in discrete time, though the continuous  
786 time version is equally tractable.

787 The problem is defined by a recursive optimality equation for the value function  $V(s|t)$   
788 in which the highest of the action values,  $Q(s, a|t)$ , is selected. We formalize the non-  
789 stationarity within episodes by conditioning on the trial time,  $t$ , where  $t = 0$  is the trial start  
790 time.  $Q(s, a|t)$  is the action-value function of average-reward reinforcement learning [11], i.e.  
791 the expected sum of future reward deviations from the average when selecting action  $a$  when  
792 in state  $s$ , at possible decision time  $t$  within a trial, and then following a given action policy  
793  $\pi$  thereafter. The action set for these binary decision tasks consists of *report left* ( $-$ ), *report*  
794 *right* ( $+$ ), and *wait*. When *wait* is selected, time increments and beliefs are updated with  
795 new evidence. We use a decision-time conditioned, expected trial reward function,  $r(s, a|t)$   
796 with  $a = \pm$ , that denotes the reward expected to be received at the end of the trial after  
797 having reported  $\pm$  in state  $s$  at time  $t$  during the trial. Note that  $r(s, a|t)$  can be defined  
798 in terms of a conventional reward function  $r(s, a)$  if the reported action, decision time, and  
799 current time are stored as an auxiliary state variable so they can be used to determine the  
800 non-zero reward entries at the end of the trial.

801 The average-reward formulation of  $Q(s, a|t)$  naturally narrows the problem onto deter-  
802 mining decisions within only a single episode of the task. To see this, we pull out the  
803 contribution of the current trial,

$$Q(s, a|t) = \mathbb{E}^{\pi} \left[ \sum_{t'=t}^T R_{t'} - \rho \left| S_t = s, A_t = a \right. \right] + V(s|T + 1) \quad (20)$$

804 where  $T$  is the (possibly stochastic) trial end time and  $V(s|T + 1)$  is the state value at the  
 805 start of the following trial, which does not depend on  $s_t$  and  $a_t$  for independently sampled  
 806 trials. Following conventional reinforcement learning notation, the expectation  $\mathbb{E}^\pi$  is over  
 807 all randomness conditioned on following the policy,  $\pi$ , which itself could be stochastic [11].  
 808 When trials are identically and independently sampled, the state at the trial start is the  
 809 same for all trials and denoted  $s_0$  with value  $V_0$ . Thus, the value at the start of the trial  
 810  $V(s|t = 0) = V(s|T+1) = V_0$  equals that at the start of the next trial and so, by construction,  
 811 the expected trial return (total trial rewards minus trial costs) must vanish (we will show  
 812 this explicitly below). Note that the value shift invariance of eq. (20) can be fixed so that  
 813  $V_0 = 0$ .

814 The *optimality equation* for  $V(s|t)$  arises from a greedy action policy over  $Q(s, a|t)$ : it  
 815 selects the action of the largest of  $Q(s, -|t)$ ,  $Q(s, +|t)$ , and  $Q(s, wait|t)$ . The value expression  
 816 for the wait-action is incremental, and so depends on the value at the next time step. In  
 817 contrast, expression for the two reporting actions integrates over the remainder of the trial  
 818 since no further decision is made and so depends on the value at the start of the following  
 819 trial. The resulting optimality equation for the value function  $V(s|t)$  is then

$$\begin{aligned}
 V(s|t) &= \max_a Q(s, a|t) , \\
 Q(s, \pm|t) &= r(s, \pm|t) - \sum_{t'=t+1}^T c_{t'} + V(s|t = T + 1) , \\
 Q(s, wait|t) &= -c_t + \mathbb{E}_{s_{t+1}|s} [V(s_{t+1}|t + 1)] , \\
 V(s|t = 0) &= V(s|t = T + 1) .
 \end{aligned}
 \tag{21}$$

820 Here,  $t = 0, 1, \dots, t_{\max}$  within the current trial and  $t = T + 1, T + 2 \dots$  in the following  
 821 trial, with  $t_{\max}$  the latest possible decision time in a trial, and  $T = T(t)$  the decision-time  
 822 dependent trial duration. For inter-trial interval  $T_{ITI}$ ,  $T$  satisfies  $T_{ITI} \leq T \leq t_{\max} + T_{ITI}$ .  
 823  $c_t$  is the cost rate at time  $t$ . The second term in  $Q(s, wait|t)$  uses the notation  $\mathbb{E}_{x|y}[z]$ , i.e.  
 824 the expectation of  $z$  with respect to  $p(x|y)$ . The last line in eq. (21) is the self-consistency  
 825 criterion imposed by the AR-RL formulation, which demands that the expected value at  
 826 the beginning of the trial be the expected value at the beginning of the following trial. The  
 827 greedy policy then gives a single decision time for each state trajectory as the first time when  
 828  $Q(s, -|t) > Q(s, wait|t)$  or  $Q(s, +|t) > Q(s, wait|t)$ , with the reporting action determined  
 829 by which of  $Q(s, -|t)$  and  $Q(s, +|t)$  is larger. For given  $c_t$ , dynamic programming provides  
 830 a solution to eq. (21) [7] by recursively solving for  $V(s|t)$  by back-iterating in time from the  
 831 end of the trial. For most relevant tasks, to never report is always sub-optimal, so the value  
 832 at  $t = t_{\max}$  is set by the best of the two reporting ( $\pm$ ) actions, which do not have a recursive  
 833 dependence on the value and so can seed the recursion.

834 We now interpret this general formulation in terms of opportunity costs. For the choice  
 835 of a static opportunity cost rate of time,  $c_t = \rho$ . This is the AR-RL case. As in [7], a  
 836 constant auxiliary deliberation cost rate,  $c$ , incurred only up to decision time can be added,  
 837  $c_t = \rho + c\Theta(t^{\text{dec}} - t)$ . Of course,  $\rho$  is unknown *a priori*. For this solution method, its value  
 838 can be found by exploiting the self-consistency constraint,  $V(s|t = 0) = V(s|t = T + 1)$ . This  
 839 dependence can be seen formally by taking the action value eq. (20), choosing  $a$  according



840 to  $\pi$  to obtain the state value,  $V(s|t)$ , and evaluating it for  $t = 0$ ,

$$V(s|t = 0) = \mathbb{E}_{t^{\text{dec}}} \left[ \sum_{t=0}^T R_t - \rho \right] + V(s|t = T + 1) \quad (22)$$

$$= \mathbb{E}_{t^{\text{dec}}} [r(t^{\text{dec}}) - \rho T(t^{\text{dec}})] + V(s|t = T + 1) \quad (23)$$

$$= \bar{R} - \rho \bar{T} + V(s|t = T + 1) . \quad (24)$$

841 Here,  $\bar{R} = \mathbb{E}_{t^{\text{dec}}} [r(t^{\text{dec}})]$  and  $\bar{T} = \mathbb{E}_{t^{\text{dec}}} [T(t^{\text{dec}})]$  denotes the expectations over the trial en-  
 842 semble that, when given the state sequence, transforms to an average over  $t^{\text{dec}}$ , the trial deci-  
 843 sion time, defined as when  $V(s|t)$  achieves its maximum on the state sequence,  $(s_0, \dots, s_{t_{\text{max}}})$ .  
 844 The expected trial reward function,  $r(t) := \max_{a \in \{-, +\}} r(s, a|t)$  is the expected trial reward  
 845 for deciding at  $t$ . Imposing the self-consistency constraint on eq. (24) recovers the definition  
 846  $\rho = \bar{R}/\bar{T}$ .

### 847 Asymmetric switching cost model

848 Here, we present the model component that accounts for the asymmetric relaxation  
 849 timescales after context switches. The basic assumption is that tracking a signal at a higher  
 850 temporal resolution should be more cognitively costly, so that adapting from faster to slower  
 851 environments should happen more quickly than the reverse, so as to not pay this cost un-  
 852 necessarily. We now develop this idea formally (see fig. S4).

853 Let  $T_{\text{track}}$  and  $T_{\text{sys}}$  be the timescale of tracking and of the tracked system, respectively.  
 854 One way to interpret the mismatch ratio,  $T_{\text{sys}}/T_{\text{track}}$ , is via an attentional cost rate,  $q$ .  
 855 This rate should decay with  $T_{\text{track}}$ : the slower the timescale of tracking, the lower the  
 856 cognitive cost. For simplicity, we set  $q = 1/T_{\text{track}}$  (fig. S4a). Integrating this cost rate over a  
 857 characteristic time of the system is then the tracking cost,  $Q = qT_{\text{sys}} = T_{\text{sys}}/T_{\text{track}}$ , which is  
 858 also the mismatch ratio. We propose that  $Q$  enters the algorithm via a scale factor on the  
 859 integration time of the reward filter for  $\hat{\rho}_k^{\tau_{\text{context}}}$ ,  $\tau_{\text{context}}$ . We redefine  $\tau_{\text{context}}$  as

$$\tau_{\text{context}} \leftarrow \frac{\tau_{\text{context}}}{1 + Q^\nu} , \quad (25)$$

860 where  $\nu$  is a sensitivity parameter that captures the strength of the nonlinear sensitivity of  
 861 the speed up (for  $\nu > 1$ ) or slow down (for  $\nu < 1$ ) in adaptation with the tracking cost,  
 862  $Q$  (fig. S4a shows how this timescale varies over  $Q$  for three values of  $\nu$ ). A natural choice  
 863 for  $T_{\text{sys}}$  is  $T_k$ , the trial duration. For  $T_{\text{track}}$ , we introduce the filtered estimate of the trial  
 864 duration,  $\hat{T}_k^{\tau_{\text{context}}}$  (computed using the same simple low-pass filter *c.f.* eq. (8)). Thus, the  
 865 tracking timescale adapts to the system timescale. As a result of how  $\tau_{\text{context}}$  is lowered by  $Q$   
 866 for  $\nu > 1$ , this adaptation is faster in the fast-to-slow transition relative to the slow-to-fast  
 867 transition.

### 868 Prediction for asymmetric rewards

869 Given a payoff matrix,  $\mathbf{R} = (r_{s,a})$ , where  $r_{s,a}$  is the reward for reporting  $a \in \{-, +\}$  in the  
 870 trial realization leading to  $s$ , here the sign of  $N_{t_{\text{max}}}$ , and the probability that the rightward

871 choice is correct,  $p_{n,t}^+$ , the expected reward for the two reporting actions in a trial is given  
872 by the matrix equation

$$[\langle r|a = +, n, t \rangle \quad \langle r|a = -, n, t \rangle] = [p_{n,t}^+ \quad 1 - p_{n,t}^+] \begin{bmatrix} r_{++} & r_{+-} \\ r_{-+} & r_{--} \end{bmatrix}.$$

873 Here, the corresponding reported choice is  $a^* = \operatorname{argmax}_{a \in \{-, +\}} \langle r|a, n, t \rangle$ . In this paper and  
874 in all existing tokens tasks,  $\mathbf{R}$  was the identity matrix. In this case, and for all cases where  
875  $\mathbf{R}$  is a symmetric matrix,  $\mathbf{R} = \mathbf{R}^\top$ , an equivalent decision rule is to decide based on the sign  
876 of  $N_t$ . When  $\mathbf{R}$  is not symmetric, however, this is no longer a valid substitute. Asymmetry  
877 can be introduced through the actions and the states.

878 Using an additional parameter  $\gamma$ , we introduce asymmetry via a bias for  $+$  actions that  
879 leaves the total reward unchanged by replacing the payoff matrix with

$$\mathbf{R}_{\text{asym}} = \begin{bmatrix} r_{++}(1 + \gamma) & r_{+-}(1 - \gamma) \\ r_{-+}(1 + \gamma) & r_{--}(1 - \gamma) \end{bmatrix},$$

880 The result for  $\gamma = -0.6, 0$ , and  $0.6$  is shown in [fig. S10](#). For  $\gamma > 0$  the decision boundary for  
881  $a = +$  shifts up proportional to  $\gamma$ . For  $\gamma < 0$  the decision boundary for  $a = -$  shifts down  
882 proportional to  $-\gamma$ . The explanation is that the components are set and exchange where  
883 the decision is exchanged,  $N_t = 0$  for the symmetric case. This changes to  $N_t \propto \pm\gamma$  for the  
884 asymmetric  $\gamma \neq 0$  case.

## 885 Comparing reward rates and slopes of urgency

886 Reference [17] parametrize urgency with the saturation value,  $u_\infty$ , and the half-maximum,  
887  $\tau_{1/2}$ . The initial slope is given by their ratio. We used the context-conditioned values  
888 published in Table 1 in [17] for the  $n = 70$  (no  $90^\circ$  control) dataset. The context-conditioned  
889 reward rates,  $\rho_\alpha$ , are computed as the accuracy  $\langle R \rangle_{|\alpha}$  divided by the average trial time,  $\langle T \rangle_{|\alpha}$   
890 for choice number  $\alpha \in \{2, 4\}$  as context. We computed  $\langle R \rangle_{|\alpha=2} = 0.71$  and  $\langle R \rangle_{|\alpha=4} = 0.49$ .  
891 The trial time is the sum of the response time, the added time penalty if incorrect, and the  
892 inter-trial interval. We computed the response times  $t_{\text{response}, \alpha=2} = 0.527$  and  $t_{\text{response}, \alpha=4} =$   
893  $0.725$ . While the dataset contains the response times, it does not have the latter two. The  
894 time penalty was on the order of 1 second, as was the time penalty [61]. Under those  
895 estimates, the reward rates are  $\rho_{\alpha=2} = 0.40$  and  $\rho_{\alpha=4} = 0.22$ . The ratio between slopes is  
896 1.8 and the ratio of reward rates was 2.3 giving an error of about 20%.

## 897 ACKNOWLEDGMENTS

898 We would like to acknowledge helpful discussions with Jan Drugowitsch, Becket Ebitz,  
899 and Paul Masset, and to Anne Churchland for sharing data from [17]. MPT acknowledges  
900 support from IVADO via their postdoctoral fellowship award. PC acknowledges support  
901 from NSERC Discovery Grant (RGPIN-2016-05245). GL acknowledges support from FRQS  
902 Research Scholar Award, Junior 1 (LAJGU0401-253188), NSERC Discovery Grant (RGPIN-

903 2018-04821), and the Canada CIFAR AI Chair program.

- 
- 904 [1] David I Green, “Pain-Cost and Opportunity-Cost,” *The Quarterly Journal of Economics* **8**,  
905 218–229 (1894).
- 906 [2] Vektor Dewanto, George Dunn, Ali Eshragh, Marcus Gallagher, and Fred Roosta, “Average-  
907 reward model-free reinforcement learning: a systematic review and literature mapping,”  
908 [arXiv:2010.08920 \[cs.LG\]](https://arxiv.org/abs/2010.08920).
- 909 [3] Nathaniel D Daw and David S Touretzky, “Long-term reward prediction in TD models of the  
910 dopamine system,” *Neural computation* **14**, 2567–2583 (2002).
- 911 [4] Lindsay E Hunter and Nathaniel D Daw, “Context-sensitive valuation and learning,” *Current*  
912 *Opinion in Behavioral Sciences* **41**, 122–127 (2021).
- 913 [5] Nils Kolling and Thomas Akam, “(Reinforcement?) Learning to forage optimally,” *Current*  
914 *Opinion in Neurobiology* **46**, 162–169 (2017).
- 915 [6] Yael Niv, Nathaniel D Daw, and Peter Dayan, “How fast to work : Response vigor , motivation  
916 and tonic dopamine,” in *Neural Information Processing Systems* (2005).
- 917 [7] Jan Drugowitsch, Rubén Moreno-Bote, Anne K Churchland, Michael N Shadlen, and Alexan-  
918 dre Pouget, “The Cost of Accumulating Evidence in Perceptual Decision Making,” *The Journal*  
919 *of Neuroscience* **32**, 3612 LP – 3628 (2012).
- 920 [8] A Ross Otto and Nathaniel D Daw, “The opportunity cost of time modulates cognitive effort,”  
921 *Neuropsychologia* **123**, 92–105 (2019).
- 922 [9] A Ross Otto and Eliana Vassena, “It’s all relative: Reward-induced cognitive control mod-  
923 ulation depends on context.” *Journal of Experimental Psychology: General* **150**, 306–313  
924 (2021).
- 925 [10] Germain Lefebvre, Aurélien Nioche, Sacha Bourgeois-gironde, and Stefano Palminteri, “Con-  
926 trasting temporal difference and opportunity cost reinforcement learning in an empirical  
927 money-emergence paradigm,” *Proceedings of the National Academy of Sciences* **115**, E11446  
928 LP – E11454 (2018).
- 929 [11] Richard S Sutton and Andrew G Barto, *Reinforcement learning: An introduction, 2nd ed.*,  
930 Adaptive computation and machine learning. (The MIT Press, Cambridge, MA, US, 2018)  
931 pp. xxii, 526–xxii, 526.
- 932 [12] Khimya Khetarpal, Matthew Riemer, Irina Rish, and Doina Precup, “Towards Continual  
933 Reinforcement Learning: A Review and Perspectives,” [arXiv:2012.13490 \[cs.LG\]](https://arxiv.org/abs/2012.13490).
- 934 [13] Roger Ratcliff, “A theory of memory retrieval.” *Psychological Review* **85**, 59–108 (1978).
- 935 [14] Gaurav Malhotra, David S Leslie, Casimir J H Ludwig, and Rafal Bogacz, “Time-varying  
936 decision boundaries : insights from optimality analysis,” *Psychon Bull Rev* **25**, 971–996 (2018).
- 937 [15] Jochen Ditterich, “Evidence for time-variant decision making,” *European Journal of Neuro-*  
938 *science* **24**, 3628–3641 (2006).
- 939 [16] Paul Cisek, Geneviève Aude Puskas, and Stephany El-Murr, “Decisions in Changing Con-  
940 ditions: The Urgency-Gating Model,” *The Journal of Neuroscience* **29**, 11560 LP – 11571  
941 (2009).
- 942 [17] Anne K Churchland, Roozbeh Kiani, and Michael N Shadlen, “Decision-making with multiple  
943 alternatives,” *Nature Neuroscience* **11**, 693–702 (2008).
- 944 [18] David Thura and Paul Cisek, “Deliberation and Commitment in the Premotor and Primary  
945 Motor Cortex during Dynamic Decision Making,” *Neuron* **81**, 1401–1416 (2014).

- 946 [19] David Thura, Ignasi Cos, Jessica Trung, and Paul Cisek, “Context-Dependent Urgency Influences Speed–Accuracy Trade-Offs in Decision-Making and Movement Execution,” *The Journal of Neuroscience* **34**, 16442 LP – 16454 (2014).
- 947  
948
- 949 [20] David Thura, Jean-François Cabana, Albert Feghaly, and Paul Cisek, “Unified neural dynamics of decisions and actions in the cerebral cortex and basal ganglia,” *bioRxiv* (2020), 10.1101/2020.10.22.350280.
- 950  
951
- 952 [21] David Thura and Paul Cisek, “The Basal Ganglia Do Not Select Reach Targets but Control the Urgency of Commitment,” *Neuron* **95**, 1160–1170.e5 (2017).
- 953
- 954 [22] Peter Janssen and Michael N Shadlen, “A representation of the hazard rate of elapsed time in macaque area LIP,” *Nature Neuroscience* **8**, 234–241 (2005).
- 955
- 956 [23] Satohiro Tajima, Jan Drugowitsch, and Alexandre Pouget, “Optimal policy for value-based decision-making,” *Nature Communications* **7**, 12400 (2016).
- 957
- 958 [24] Anton Schwartz, “A Reinforcement Learning Method for Maximizing Undiscounted Rewards,” in *International Conference on Machine Learning*, Vol. 0 (1993).
- 959
- 960 [25] Yael Niv, Nathaniel D Daw, Daphna Joel, and Peter Dayan, “Tonic dopamine: opportunity costs and the control of response vigor,” *Psychopharmacology* **191**, 507–520 (2007).
- 961
- 962 [26] Sara M Constantino and Nathaniel D Daw, “Learning the opportunity cost of time in a patch-foraging task,” *Cogn Affect Behav Neurosci.* **15**, 837 (2015).
- 963
- 964 [27] Benjamin Y Hayden and Yael Niv, “The case against economic values in the orbitofrontal cortex (or anywhere else in the brain),” *PsyArXiv* 10.31234/osf.io/7hgup.
- 965
- 966 [28] Nathaniel D Daw, “Advanced Reinforcement Learning,” in *Neuroeconomics*, edited by Paul W Glimcher and Ernst B T Neuroeconomics (Second Edition) Fehr (Academic Press, San Diego, 2014) 2nd ed., Chap. 16, pp. 299–320.
- 967  
968
- 969 [29] D. Thura. Personal communication.
- 970 [30] Edward Vul, Noah Goodman, Thomas L Griffiths, and Joshua B Tenenbaum, “One and Done? Optimal Decisions From Very Few Samples,” *Cognitive Science* **38**, 599–637 (2014).
- 971
- 972 [31] Single subject behavioural data shared by Thomas Thierry.
- 973 [32] Surya Ganguli, James W Bisley, Jamie D Roitman, Michael N Shadlen, Michael E Goldberg, and Kenneth D Miller, “One-Dimensional Dynamics of Attention and Decision Making in LIP,” *Neuron* **58**, 15–25 (2008).
- 974  
975
- 976 [33] David Thura and Paul Cisek, “Modulation of Premotor and Primary Motor Cortical Activity during Volitional Adjustments of Speed-Accuracy Trade-Offs,” *The Journal of Neuroscience* **36**, 938 – 956 (2016).
- 977  
978
- 979 [34] Kiyohito Iigaya, Yashar Ahmadian, Leo P Sugrue, Greg S Corrado, Yonatan Loewenstein, William T Newsome, and Stefano Fusi, “Deviation from the matching law reflects an optimal strategy involving learning over multiple timescales,” *Nature Communications* **10**, 1466 (2019).
- 980  
981
- 982 [35] Long Ding and Joshua I. Gold, “The Basal Ganglia’s Contributions to Perceptual Decision Making,” *Neuron* **79**, 640–649 (2013).
- 983
- 984 [36] Kong-Fatt Wong and Xiao-Jing Wang, “A Recurrent Network Mechanism of Time Integration in Perceptual Decisions,” *The Journal of Neuroscience* **26**, 1314 – 1328 (2006).
- 985
- 986 [37] Alex Roxin and Anders Ledberg, “Neurobiological Models of Two-Choice Decision Making Can Be Reduced to a One-Dimensional Nonlinear Diffusion Equation,” *PLOS Computational Biology* **4**, e1000046 (2008).
- 987  
988
- 989 [38] David Meder, Nils Kolling, Lennart Verhagen, Marco K Wittmann, Jacqueline Scholl, Kristoffer H Madsen, Oliver J Hulme, Timothy E J Behrens, and Matthew F S Rushworth, “Simultaneous representation of a spectrum of dynamically changing value estimates during decision
- 990  
991

- 992 making,” *Nature Communications* **8** (2017), [10.1038/s41467-017-02169-w](https://doi.org/10.1038/s41467-017-02169-w).
- 993 [39] “Predictive Representations in Hippocampal and Prefrontal Hierarchies,” .
- 994 [40] Jan Zimmermann, Paul W Glimcher, and Kenway Louie, “Multiple timescales of normalized  
995 value coding underlie adaptive choice behavior,” *Nature Communications* **9**, 3206 (2018).
- 996 [41] HyungGoo R Kim, Athar N Malik, John G Mikhael, Pol Bech, Iku Tsutsui-Kimura, Fangmiao  
997 Sun, Yajun Zhang, Yulong Li, Mitsuko Watabe-Uchida, Samuel J Gershman, and Naoshige  
998 Uchida, “A Unified Framework for Dopamine Signals across Timescales,” *Cell* **183**, 1600–  
999 1616.e25 (2020).
- 1000 [42] Paul Masset, Athar N. Malik, HyungGoo R. Kim, Pol Bech, and Naoshige Uchida, “A  
1001 diversity of discounting horizons explains ramping diversity in dopaminergic neurons,” in  
1002 *COSYNE Abstracts* (2021).
- 1003 [43] Angela J Langdon and Nathaniel D Daw, “Beyond the Average View of Dopamine,” *Trends  
1004 in Cognitive Sciences* **24**, 499–501 (2020).
- 1005 [44] John G Mikhael and Samuel J Gershman, “Adapting the flow of time with dopamine,” *Journal  
1006 of Neurophysiology* **121**, 1748–1760 (2019).
- 1007 [45] Ido Toren, Kristoffer C Aberg, and Rony Paz, “Prediction errors bidirectionally bias time  
1008 perception,” *Nature Neuroscience* **23**, 1198–1202 (2020).
- 1009 [46] Lars Hunger, X Arvind Kumar, and X Robert Schmidt, “Abundance Compensates Kinet-  
1010 ics : Similar Effect of Dopamine Signals on D1 and D2 Receptor Populations,” *Journal of  
1011 Neuroscience* **40**, 2868–2881.
- 1012 [47] Julia Cox and Ilana B Witten, “Striatal circuits for reward learning and decision-making,”  
1013 *Nature Reviews Neuroscience* **20**, 482–494 (2019).
- 1014 [48] Helen N Schwerdt, Hideki Shimazu, Ken-ichi Amemori, Satoko Amemori, Patrick L Tierney,  
1015 Daniel J Gibson, Simon Hong, Tomoko Yoshida, Robert Langer, Michael J Cima, and Ann M  
1016 Graybiel, “Long-term dopamine neurochemical monitoring in primates,” *Proceedings of the  
1017 National Academy of Sciences* **114**, 13260 LP – 13265 (2017).
- 1018 [49] Tommaso Patriarchi, Jounhong Ryan Cho, Katharina Merten, Mark W Howe, Aaron Marley,  
1019 Wei-hong Xiong, Robert W Folk, Gerard Joey Broussard, Ruqiang Liang, Min Jee Jang,  
1020 Haining Zhong, Daniel Dombeck, Mark Von Zastrow, Axel Nimmerjahn, Viviana Gradinaru,  
1021 John T Williams, and Lin Tian, “Ultrafast neuronal imaging of dopamine dynamics with  
1022 designed genetically encoded sensors,” *Science* **4422** (2018), [10.1126/science.aat4422](https://doi.org/10.1126/science.aat4422).
- 1023 [50] Matthew A Carland, David Thura, and Paul Cisek, “The Urge to Decide and Act: Implica-  
1024 tions for Brain Function and Dysfunction,” *The Neuroscientist* **25**, 491–511 (2019).
- 1025 [51] Samuel J Gershman and Naoshige Uchida, “Believing in dopamine,” *Nature Reviews Neuro-  
1026 science* **20**, 703–714 (2019).
- 1027 [52] Andrew Westbrook and Todd S Braver, “Dopamine Does Double Duty in Motivating Cognitive  
1028 Effort,” *Neuron* **91**, 708 (2016).
- 1029 [53] Pablo Tano, Peter Dayan, and Alexandre Pouget, “A Local Temporal Difference Code for  
1030 Distributional Reinforcement Learning,” in *Advances in Neural Information Processing Sys-  
1031 tems*, Vol. 33, edited by H Larochelle, M Ranzato, R Hadsell, M F Balcan, and H Lin (Curran  
1032 Associates, Inc., 2020) pp. 13662–13673.
- 1033 [54] William Fedus, Carles Gelada, Yoshua Bengio, Marc G Bellemare, and Hugo Larochelle,  
1034 “Hyperbolic Discounting and Learning over Multiple Horizons,” [arXiv:1902.06865 \[stat.ML\]](https://arxiv.org/abs/1902.06865).
- 1035 [55] I Momennejad, E M Russek, J H Cheong, M M Botvinick, N D Daw, and S J Gershman,  
1036 “The successor representation in human reinforcement learning,” *Nature Human Behaviour*  
1037 **1**, 680–692 (2017).

- 1038 [56] Personal communication, Thomas Thierry.
- 1039 [57] Stefano Palminteri and Maël Lebreton, “Context-dependent outcome encoding in human re-  
1040 inforcement learning,” *Current Opinion in Behavioral Sciences* **41**, 144–151 (2021).
- 1041 [58] Ernest S Davis and Gary F Marcus, “Computational limits don’t fully explain human cognitive  
1042 limitations,” *Behavioral and Brain Sciences* **43**, e7 (2020).
- 1043 [59] Arman Abrahamyan, Laura Luz Silva, Steven C Dakin, Matteo Carandini, and Justin L Gard-  
1044 ner, “Adaptable history biases in human perceptual decisions,” *Proceedings of the National  
1045 Academy of Sciences* **113**, E3548 LP – E3557 (2016).
- 1046 [60] Zhijian Wang, Bin Xu, and Hai-Jun Zhou, “Social cycling and conditional responses in the  
1047 Rock-Paper-Scissors game,” *Scientific Reports* **4**, 5830 (2014).
- 1048 [61] A. Churchland. Personal communication.



1049

## Supplemental Materials

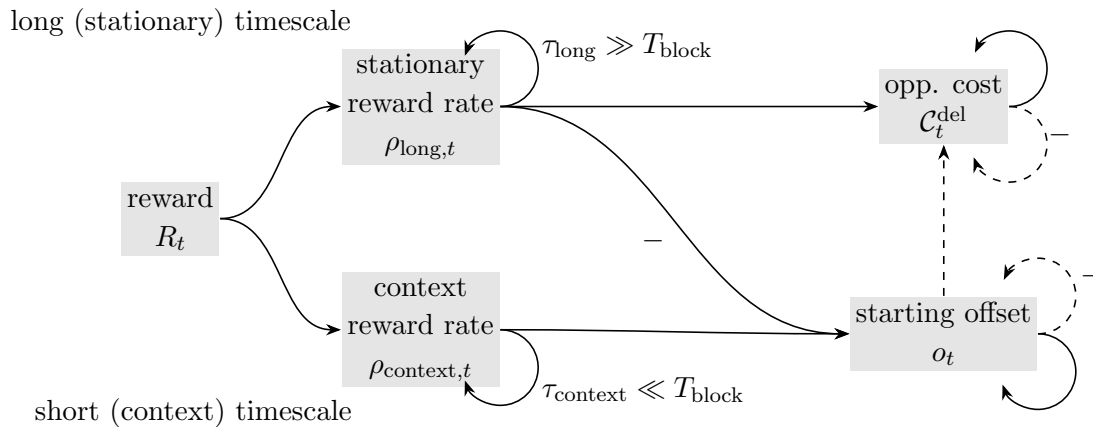


Figure S1. *Reward filtering scheme for online computation of within-trial opportunity cost.* With  $t$  denoting absolute time, the reward sequence,  $R_t$ , is integrated on both a stationary ( $\tau_{\text{long}}$ ) and context ( $\tau_{\text{context}}$ ) filtering timescale to produce estimates of the stationary and context-specific reward rates, respectively. These are large and small, respectively, relative to the average context switching timescale,  $T_{\text{block}}$ . The estimate of the context-specific offset,  $o_t$  is computed by time-integrating the difference of these two estimates. In this filtering, when a trial terminates, the effective operation is that  $C_t^{\text{del}}$  is set to  $o_t$ , and the latter is zeroed. Thus, the opportunity cost starts at this offset and then integrates  $\rho_{\text{long}}$ ,  $C_{t,k}^{\text{del}} = o_{T_{k-1},k-1} + \rho_{\text{long},k-1}t$ , where  $o_{T_{k-1},k-1} = (\rho_{\text{context},k-1} - \rho_{\text{long},k-1})T_{k-1}$ . Notes on the computational graph: Arrows pass the value at each time step (dashed arrows only pass the value when a trial terminates). Links annotated with ‘-’ multiply the passed quantity by  $-1$ .

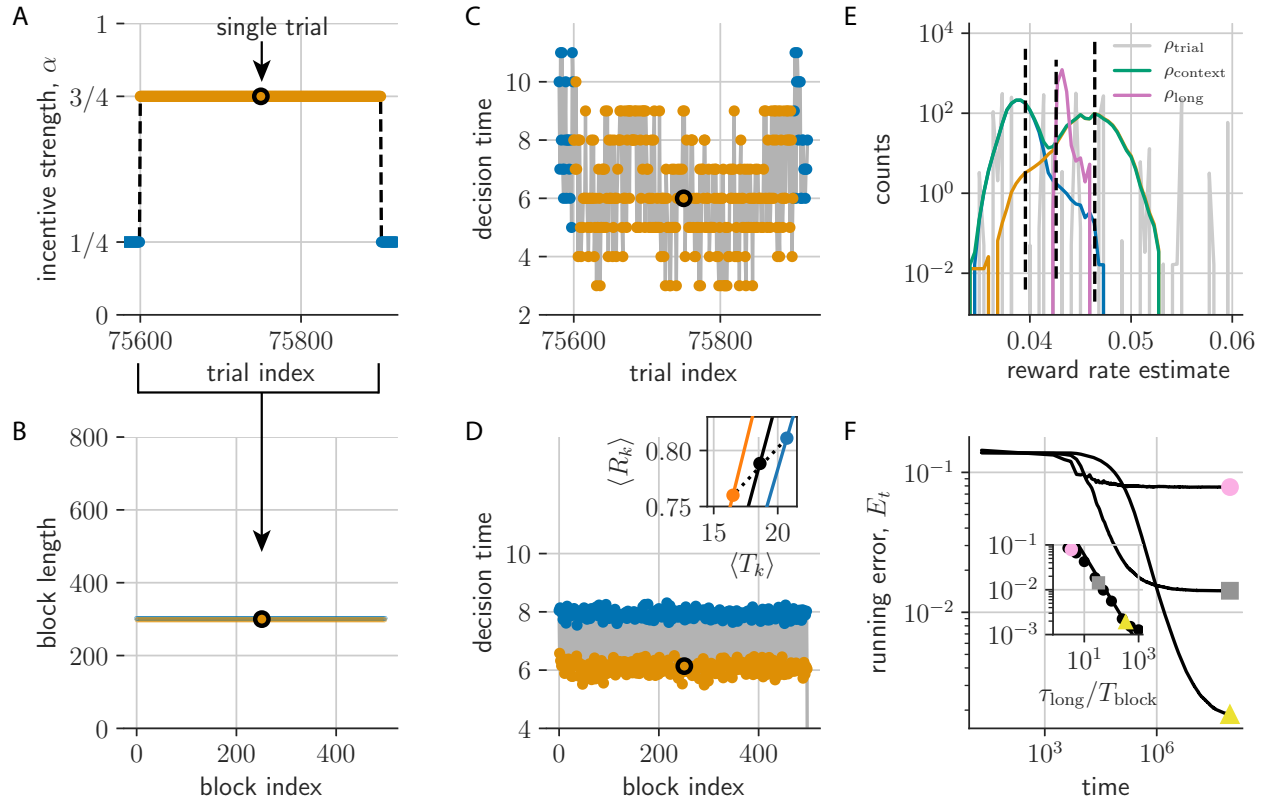


Figure S2. *PGD agent plays the tokens task with periodic  $\alpha$ -dynamics.* (a) Trials are grouped into alternating trial blocks of constant  $\alpha$  (fast (orange) and slow (blue) conditions). (b) Here, trial block durations are constant over the experiment. (c) Decision times over the trials from (a) distribute widely, but relax after context switches. (d) Block-averaged decision times remain stationary. Inset shows the context-conditioned trial-averaged reward  $\langle R_k \rangle$  and trial duration  $\langle T_k \rangle$  (orange and blue dots; black is unconditioned average;  $\langle \cdot \rangle$  denotes the trial ensemble average). Lines pass through the origin (slope given by the respective reward rate). (e) Distribution of estimates have lower variance than the trial reward rates,  $\rho^{\text{trial}}$  (gray). The conditioned averages of  $\hat{\rho}_k^{\text{context}}$  shown as blue and orange. (f) The relative error in estimating  $\rho$ ,  $E_t = \frac{1}{t} \sum_k^t |\hat{\rho}_k^{\tau_{\text{long}}} - \rho| / \rho$ , for  $\tau_{\text{long}} = 10^3$  (circle),  $10^4$  (square),  $10^5$  (triangle). Inset shows that  $E_{T_{\text{exp}}} \propto (\tau_{\text{long}}/T_{\text{block}})^{-1}$  over a grid of  $\tau_{\text{long}}$  and  $T_{\text{block}}$  as expected (black line).

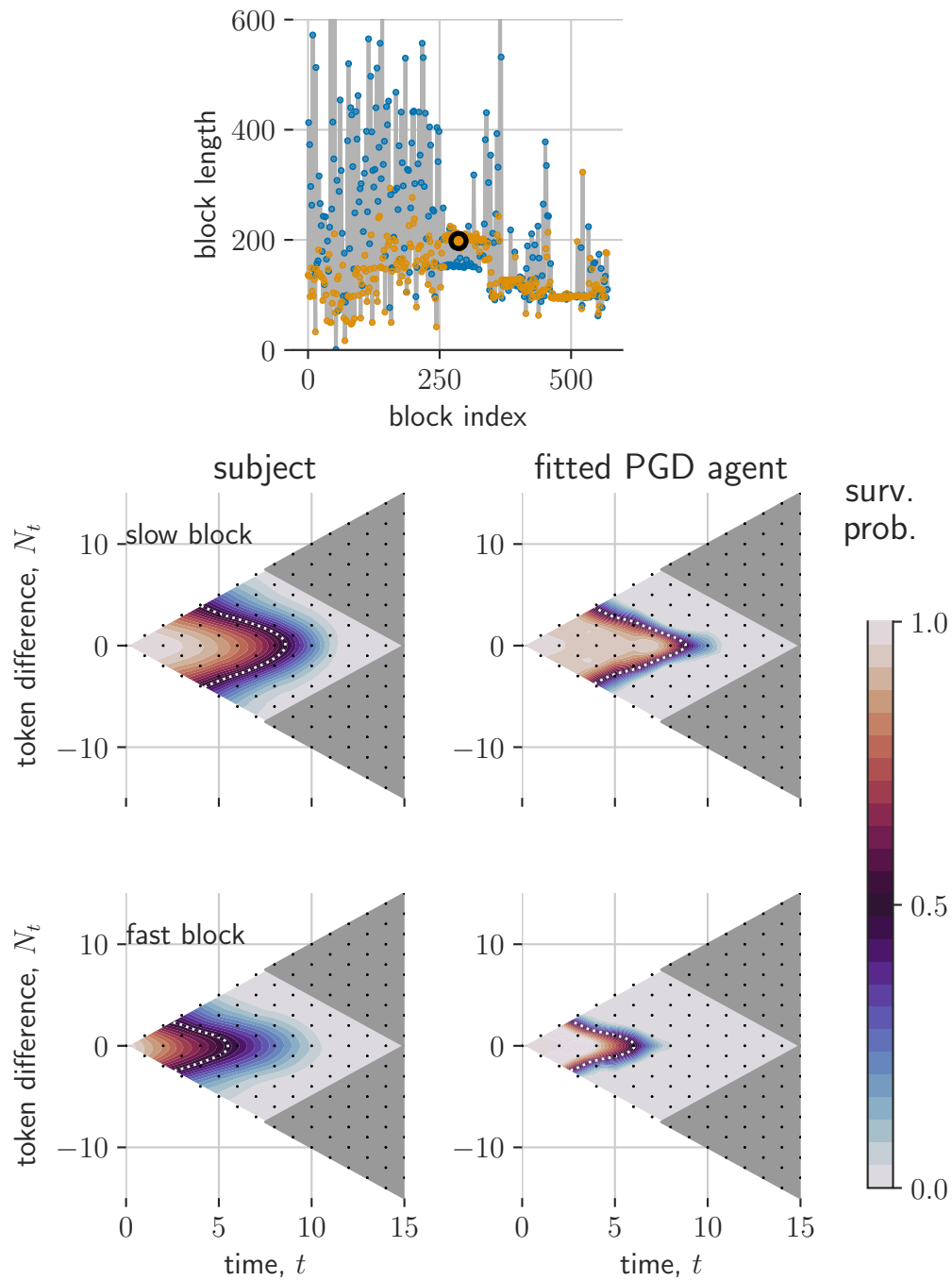


Figure S3. Comparison of PGD and NHP in non-stationary  $\alpha$  dynamics from [19]: Subject 2. Same as fig. 5.

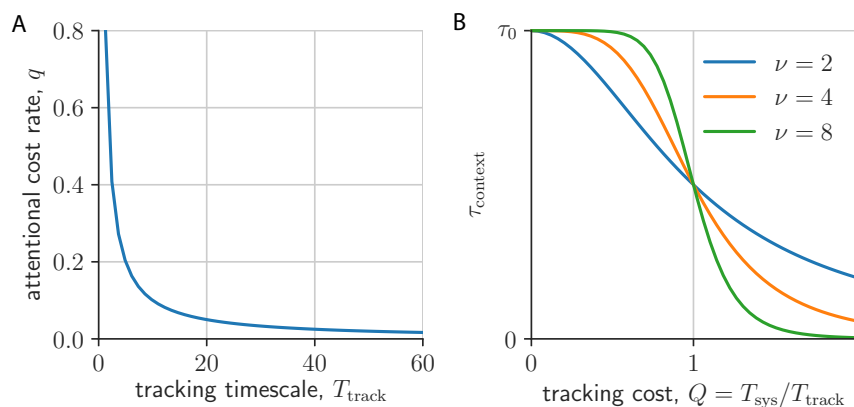


Figure S4. *Asymmetric switching cost model*. (a) Attentional cost rate,  $q$ , is set to be inversely proportional to tracking timescale,  $T_{\text{track}}$ . (b) Filtering timescale  $\tau_{\text{context}}$  is scaled down with tracking cost,  $Q = T_{\text{sys}}/T_{\text{track}}$  from a base timescale, here denoted  $\tau_0$  (shown for three values of sensitivity  $\nu = 2, 4, 8$ ).

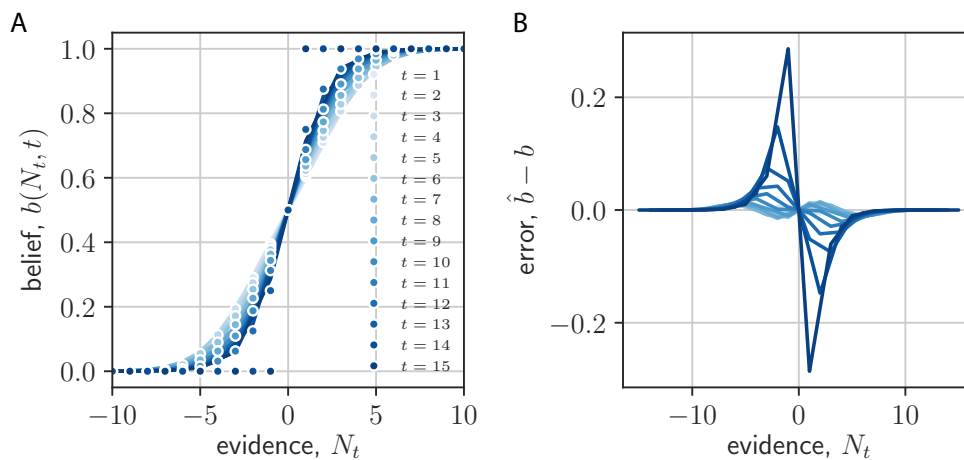


Figure S5. *sigmoidal approximation to expected reward*. (a) the approximation explained in [Methods: State-conditioned expected trial reward](#), for different dec,[p]ision times. (b) The error in the approximation for different decision times.

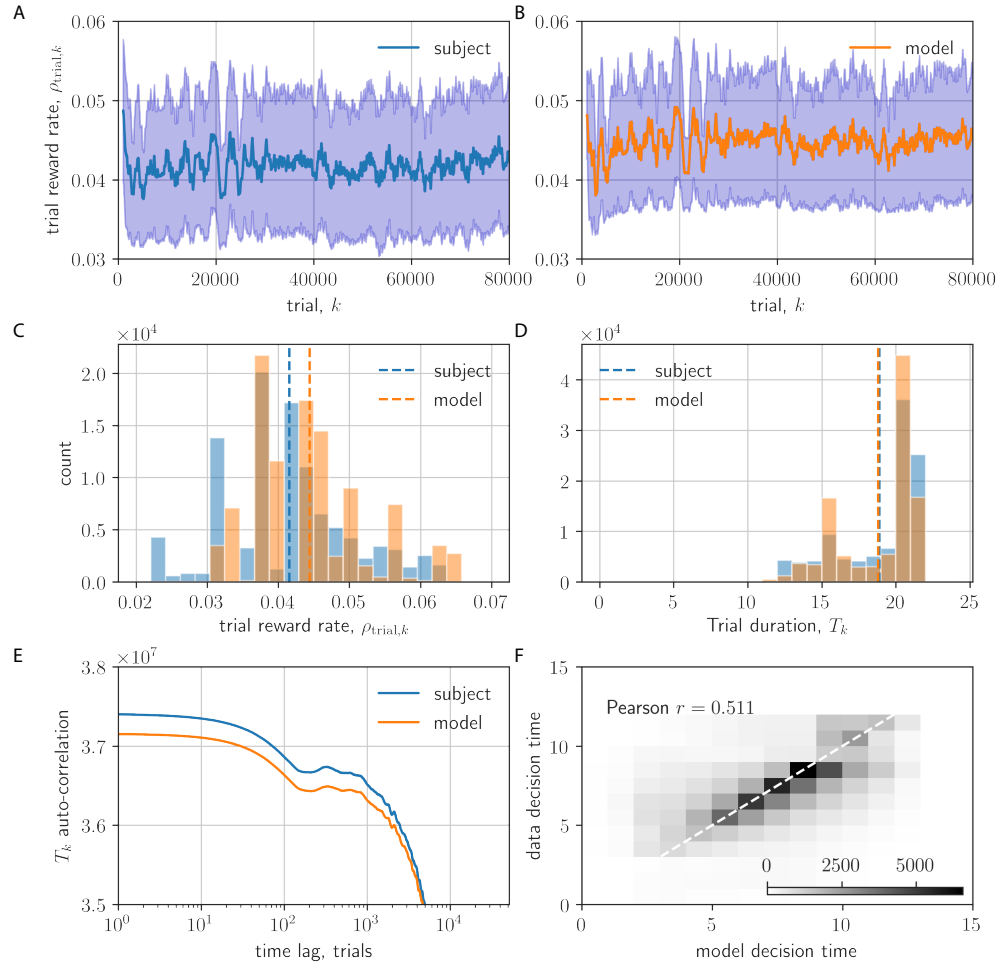


Figure S6. *Model validation on behavioural statistics from [19].* (a,b) Running average (last 1000 trial) of trial reward rate  $\rho_k^{\text{trial}}$ . (c,d) Histograms of trial reward rate,  $\rho_k^{\text{trial}}$  (c) and trial duration,  $T_k$  (d). (e) Auto-correlation function of trial duration. (f) Data vs. model decision time (gray-scale is count; white dashed line is perfect correlation; actual Pearson correlation is shown)



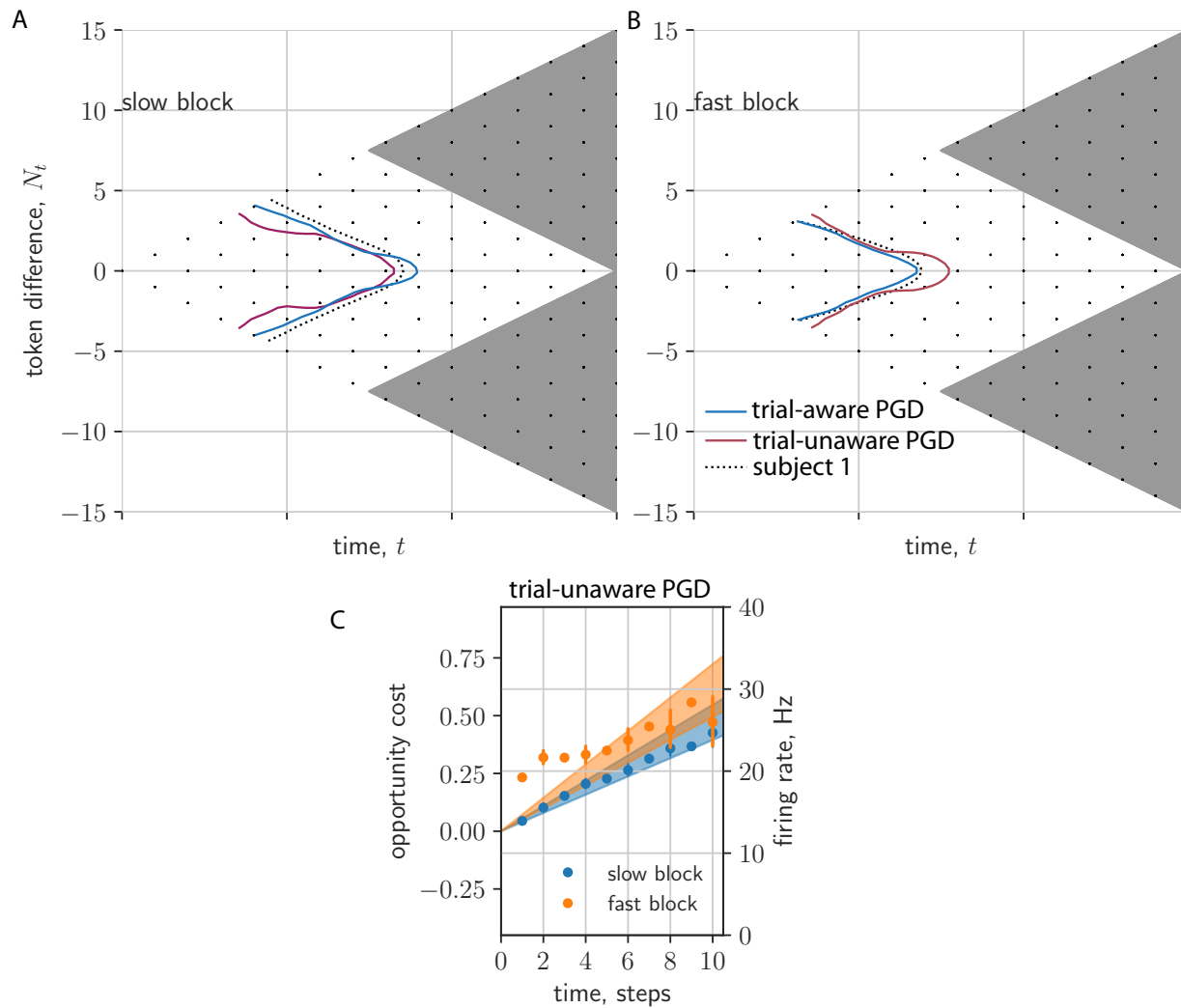


Figure S7. *Comparison of trial-aware and trial-unaware results.* (a,b) 1/2-Survival probability contours for subject 1 (dashed), trial-aware PGD (blue), and trial-unaware PGD (red) for slow (a) and fast (b) context-conditioned data. (c) Opportunity cost for trial-unaware PGD (compare with [fig. 2b](#)). Opportunity cost range adjusted here such that data within standard error of trial-unaware PGD model prediction for slow block (blue).

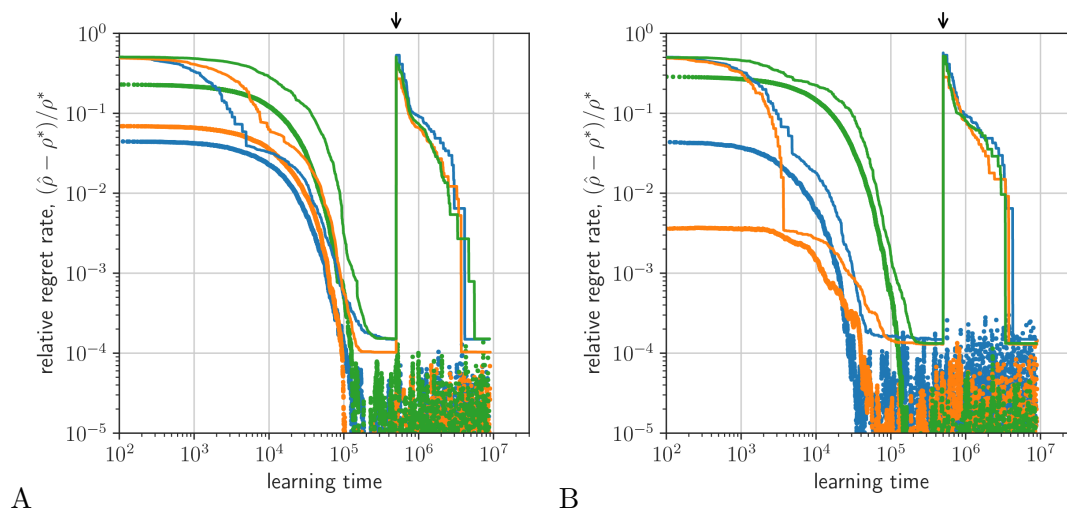


Figure S8. *Comparison of PGD and AR-RL learning on a patch leaving task.* Performance is defined as relative regret rate,  $(\hat{\rho} - \rho^*)/\rho^*$  (PGD (dots); AR-RL (lines)). (a) Performance over different sizes of the state vector ( $d = 100$  (blue),  $200$  (orange),  $300$  (green)). (b) Performance over different learning rates (parametrized by integration time constant,  $\tau = 1 \times 10^4$  (blue),  $2 \times 10^4$  (orange),  $3 \times 10^4$  (green)). (parameters:  $\lambda = 1/5$ ;  $r_{\max}$  sampled uniformly on  $[0, 1]$ ). A random state label permutation is made at the time indicated by the black arrow. Values were initialized at  $-1$ .

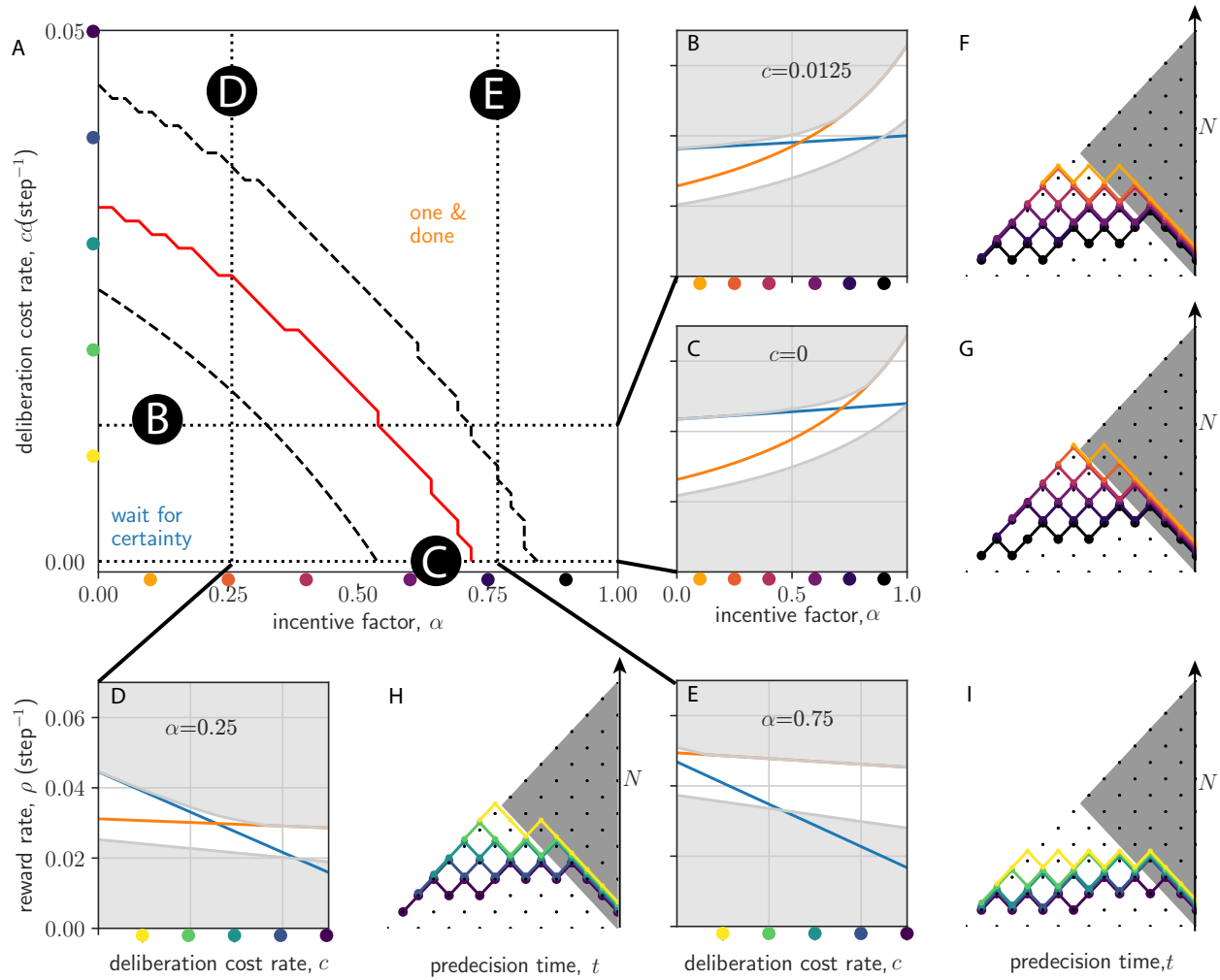


Figure S9. *Reward rate optimal strategies in  $(\alpha, c)$  plane.* (a) The reward-rate maximizing policy interpolates from the wait-for-certainty strategy at weak incentive (low  $\alpha$ ) and low deliberation cost (low  $c$ ), to the one-and-done strategy at strong incentive (high  $\alpha$ ) and high deliberation cost (high  $c$ ). Dashed lines bound a transition regime between the two extreme strategies. Red line denotes where they have equal performance. (b-e) Slices of the  $(\alpha, c)$ -plane. Shown are the reward rate as a function of  $\alpha$  (b,c) and  $c$  (d,e) (wait-for-certainty strategy is shown in blue; one-and-done strategy is shown in orange).  $N$  is the magnitude of the token difference

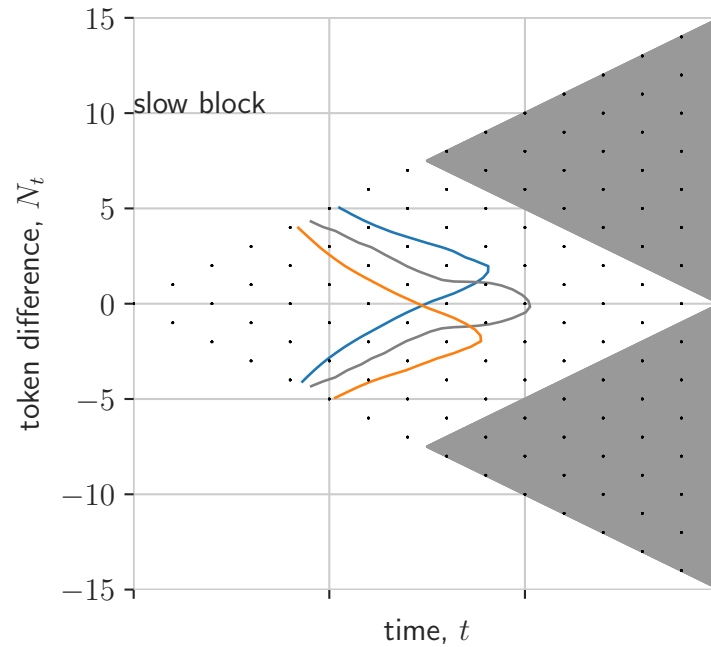


Figure S10. *Asymmetric action rewards skew survival probability.* Here, we plot the half-maximum of the PGD survival probability for three values of the action reward bias,  $\gamma = -0.6, 0, 0.6$  (blue, black and orange, respectively). Other model parameters same as in fitted model.

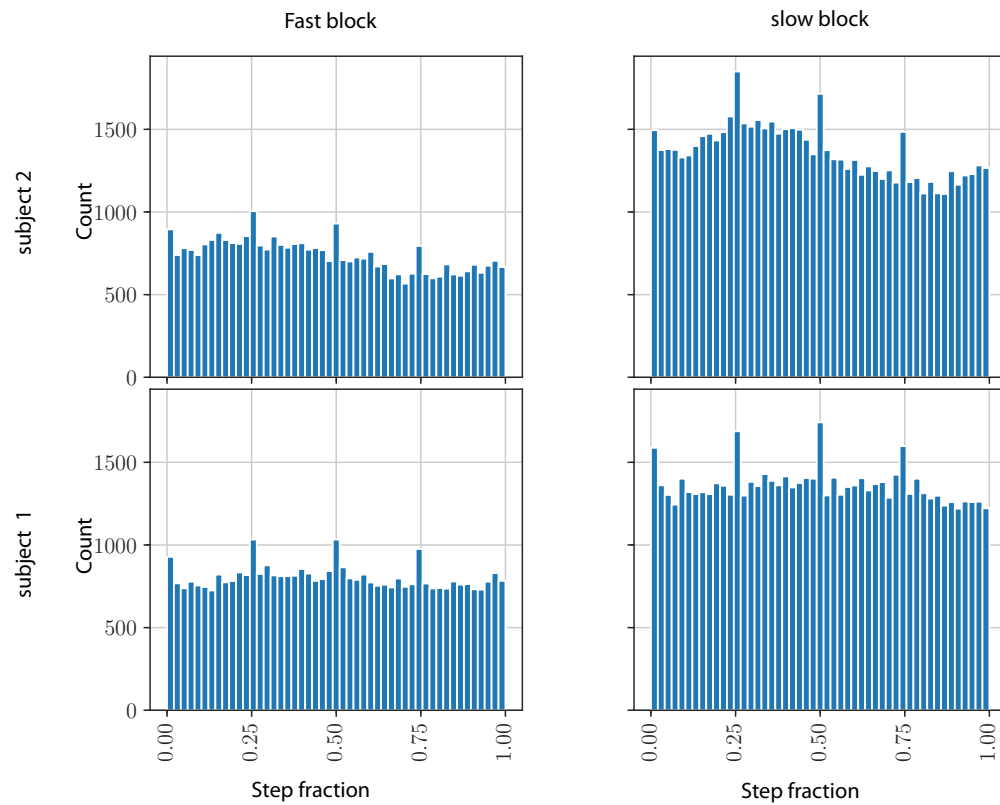


Figure S11. *Decision times relative to token jumps.* Here, we plot the histograms of decision times using their position between token jumps, the step fraction. The data is separated by  $\alpha$  and monkey.